AD-A266 474



DTIC
ELECTE
JUL 6 1993
S C D

ARMY RESEARCH LABORATORY

Wear Resistant Titanium Material Development

D. G. Konitzer, N. O. Maurer, and
K. P. Taylor

ARL-CR-51 March 1993

prepared by

GE Aircraft Engines
1 Neumann Way
Cincinnati, OH 45215-6301

under contract

DAAL04-91-C-0036

93-15193



Approved for public release; distribution unlimited.

The findings in this report are not to be construed as an official Department of the Army position unless so designated by other authorized documents.

Citation of manufacturer's or trade names does not constitute an official endorsement or approval of the use thereof.

Destroy this report when it is no longer needed. Do not return it to the originator.

REPORT DOCUMENTATION PAGE

Form Approved
OMB No. 0704-0188

Public reporting burden for this collection of information is estimated to average 1 hour per response, including the time for reviewing instructions, searching existing data sources, gathering and maintaining the data needed, and completing and reviewing the collection of information. Send comments regarding this burden estimate or any other aspect of this collection of information, including suggestions for reducing this burden, to Washington Headquarters Services, Directorate for Information Operations and Reports, 1215 Jefferson Davis Highway, Suite 1204, Arlington, VA 22202-4302, and to the Office of Management and Budget, Paperwork Reduction Project (0704-0188), Washington, DC 20503

1. AGENCY USE ONLY *(Leave blank)*	2. REPORT DATE	3. REPORT TYPE AND DATES COVERED
	March 1993	Final Report - 10/1/91 - 9/30/92

4. TITLE AND SUBTITLE
Wear Resistant Titanium Material Development

5. FUNDING NUMBERS
DAAL04-91-C-0036

6. AUTHOR(S)
D. G. Konitzer, N. O. Maurer, and K. P. Taylor

7. PERFORMING ORGANIZATION NAME(S) AND ADDRESS(ES)
GE Aircraft Engines
1 Neumann Way
Cincinnati, OH 45215-6301

8. PERFORMING ORGANIZATION REPORT NUMBER

9. SPONSORING/MONITORING AGENCY NAME(S) AND ADDRESS(ES)
U.S. Army Research Laboratory
Watertown, MA 02172-0001
ATTN: AMSRL-OP-PR-WT

10. SPONSORING/MONITORING AGENCY REPORT NUMBER
ARL-CR-51

11. SUPPLEMENTARY NOTES
Martin G. H. Wells, COR

12a. DISTRIBUTION/AVAILABILITY STATEMENT
Approved for public release; distribution unlimited.

12b. DISTRIBUTION CODE

13. ABSTRACT *(Maximum 200 words)*

A method for producing a dispersion of a hard phase in a titanium alloy is being studied. The purpose of the hard phase, titanium carbide in this work, is to improve the wear and erosion resistance of the titanium matrix. The hard phase has been produced in a wide range of volume fractions by nonconsumable arc melting.

14. SUBJECT TERMS
Titanium, Wear, Titanium carbide, Hard phase, Erosion

15. NUMBER OF PAGES
35

16. PRICE CODE

17. SECURITY CLASSIFICATION OF REPORT	18. SECURITY CLASSIFICATION OF THIS PAGE	19. SECURITY CLASSIFICATION OF ABSTRACT	20. LIMITATION OF ABSTRACT
Unclassified	Unclassified	Unclassified	UL

NSN 7540-01-280-5500

Standard Form 298 (Rev. 2-89)
Prescribed by ANSI Std. Z39-18
298-102

Table of Contents

1.0 Program Objective and Scope	1
2.0 Results	1
Small Ingots	1
Large Ingots	2
Wear and Erosion	5
3.0 Summary and Conclusions	6
4.0 Future Recommendations	6
5.0 References	6

1.0 PROGRAM OBJECTIVE AND SCOPE

This program explored the feasibility of producing a Ti based alloy with improved wear and erosion resistance compared to present Ti alloys. The need for these alloys is based on the fact that Army engines operate close to the ground where airborne particles are ingested into the engines. The recent Desert Storm experience indicates that materials with improved wear and erosion resistance would benefit the Army. The approach to achieving the wear and erosion improvement was to incorporate a dispersion of hard particles within the matrix by conventional processing routes. The program was broken into two phases; the first phase being a study of the relationships among volume fraction of hard phase, wear / erosion resistance and mechanical properties. The second phase was to be a demonstration of the relationships found in phase 1 on scaled up ingots . Phase 1 was funded, while phase 2 was not funded, therefore, this report covers the efforts performed under phase 1.

The program was supported by the U.S. Army Research Laboratory, Materials Directorate, Dr. Martin Wells was the program monitor. The effort was carried out by GE Aircraft Engines where Dr. Douglas Konitzer was the program manager.

2.0 Results

Small Ingots

The matrix alloy was chosen to be 50.5Ti-40.5Nb-9Al, atomic percent. This alloy has been demonstrated to have ductilities at room temperature of up to 30% elongation (*1*). The properties of the alloy can be changed significantly through thermal treatments, therefore, this alloy composition allows the properties of the matrix to be varied, such that the expected tradeoff between ductility and volume fraction of hard phase can be studied. The five aim screening compositions produced and measured densities are listed in tables 3.1 and 3.2. Small specimens of the screening alloys were produced by nonconsumable arc melting in a copper hearth. Each button was inverted and remelted a minimum of five times to ensure homogeneity. Alloy 1 was chosen as a control while the other four were chosen to produce an increasing volume fraction of hard phase.

The five alloys were given three heat treatments, 1050°C (1925°F) / 24 h, 1200°C (2200°F) / 24h, and 1350°C (2425°F) / 4 h to determine the effect of heat treatment on the hard particle dispersion. The microstructures for the various compositions and heat treatments are shown in figures 3.1-3.5. All three heat treatments resulted in precipitation of a plate-like second phase within the carbides. Energy dispersive spectroscopy indicated these precipitates have compositions very similar to the matrix. Therefore, it is believed that the plates are the parent matrix phase which precipitates in the carbide particles. The carbide reinforcements became more spherodized as the temperature increased.

Image analysis was utilized to determine the carbide volume fraction as a function of carbon content and solution heat treat temperature for a given alloy. The relationship between volume fraction of carbide and atomic percent of carbon in the alloys studied is linear, Figure 3.6, and has a slope of 2.

for
CRA&I
TAB
nounced
ication
By
Distribution /
Availability Codes
Dist | Avail and / or Special
A-1

DTIC

Electron microprobe analysis was performed on each solution treated specimen and the results are presented in Table 3.3. Carbon content cannot be determined due to equipment limitations. Therefore, it was presumed that the remaining element required to sum to 100% is C. From the data it can be concluded that the composition of the stable carbide is approximately Ti_2C. It was observed, Table 3.3, that after the 1050°C / 24 h solution treatment the carbide niobium concentration increases and the carbide titanium concentration decreases with increases in alloy carbon content, Figure 3.7. This variation in the composition indicates that the carbide composition is more accurately $(Ti,Nb)_2C$. It should be noted that the Nb/Ti ratio in the alloys is constant for all carbon contents. The composition analysis was performed on all specimens only for the 1050°C heat treatment, although presumably a similar effect would be seen for the other heat treatments. The carbide aluminum and carbon concentration stay relatively constant for alloys 1 - 5 after 1050°C / 24 h.

Transmission electron microscopy was utilized to determine the carbide as being of a structure similar to that of Ti_2C. The diffuse streaking observed in the [101] zone axis pattern, Figure 3.8, of the Ti carbide is consistent with that required in the [101] zone axis of Ti_2C (2). Therefore, the hard phase in these alloys is determined to be $(Ti,Nb)_2C$

Large Ingots

The materials for mechanical and wear / erosion testing were cast and forged at GE Corporate Research & Development Center. The forgings were produced from 7.6 cm diameter by 6.4 cm high sections removed from the middle of ingots as shown in figure 3.9. These ingots were reduced by 80% in height in two steps, each 50% of the total deformation, at 1100°C.

As can be seen in Figure 3.10, no edge cracking or other significant forging defects were generated. The forged pancakes, for the five alloys, exhibited varying surface texture along the pancake edges, Figure 3.10. Alloy 5, with a high carbide volume fraction, had a very smooth edge whereas alloy 1 had significant grain texture. Grain size in alloy 5 was measured to be 15 microns compared to the alloy 1 grain size of 900 microns. The as-cast microstructure of the alloys consisted of carbides, Figure 3.11, and a single phase matrix. The carbides in the lower carbon alloys line the grain boundaries whereas the higher carbon alloys contain spheroidal carbides along the grain boundary with a few dendritic carbides. It was found that alloy 5, the highest carbon alloy, contained undissolved carbon particles from the melt. These inclusions were expected to reduce some of the mechanical properties.

Two process routes were investigated, Table 3.4. Process one consists of forging of the cast ingot followed by thermal treatment (1350°C / 4 hr) to spherodize the carbide with subsequent aging treatments to produce matrix precipitation. Process two consists of thermal treatment of the cast ingot to produce carbide spherodization followed by forging with subsequent thermal treatments of either direct age or solution / anneal (1250°C / 4 hr) + age, to produce the matrix microstructure. Different carbide morphologies and distributions

were expected to result from the two process routes. With process one the needle/plate carbides were expected to be broken down during the forging process and spherodized by the subsequent solution / anneal treatment with a resulting finer carbide size. With process two, however, much of the spherodizing was expected to occur during the initial thermal treatment, resulting in larger carbides with a narrower size distribution following forging, which was not expected to have much effect on the spherodized carbides.

Figures 3.12 and 3.13 show the microstructure of the alloy prior to forging, i.e. forge preheat only for process one and 1350°C/4h plus forge preheat for process two. These figures show the effect of the thermal cycle only and not the deformation. The microstructure in both figures shows some carbide spherodization and grain growth. The material which received the process two treatment was somewhat more spherodized than the material which underwent the process one forge thermal cycle (1100°C / 0.5h) only. Low carbon alloys showed the effect of the difference in the two process routes more so than the high carbon alloys.

Figure 3.14 is representative of the microstructure following the forge + 1350°C / 4 hr solution treatment of process one, and Figure 3.15 shows the microstructures generated by 1350°C / 4 hr solution treatment + forging of process two. These figures show that the lower carbon alloys, for process two, have elongated carbide morphologies and a bimodal carbide size distribution compared to the spherical morphology and uniform size distribution seen in process one specimens. In general carbide morphology was more spherodized following process one than process two, while the carbides were larger following process two.

The heat treatment response of the five alloys was different for the two processes, because of the difference in material condition going into the heat treatment, i.e. process one was solution treated at 1350°C while process two material was as deformed. The heat treat conditions studied for both process routes were based on results from similar alloys (3) and ranged from 600 to 800°C for 24 and 50 hr times. Scanning electron microscope backscatter images of the various aged structures obtained for process one are shown in Figures 3.16 through 3.20. The matrix precipitation is of a lath morphology and appears to be coarser with increased aging temperature while, what appear to be precipitate free zones are present at the grain boundaries at the lower aging temperatures. X-ray diffraction could only reveal that the precipitation was either alpha-Ti or orthorhombic in the sample studied, due to too low a volume fraction i.e. low intensities. Previous work (4) performed on similar alloys, without carbon, indicates that this phase is most likely an orthorhombic structure of Ti_2AlNb stoichiometry.

Process two specimens have two heat treatment options following the forging, direct age or solution / anneal + age. The process two specimens which were direct aged at 700°C / 24 hr after forging resulted in a more homogeneous dispersion of matrix precipitation than the process one specimens which were solution treated at 1350°C / 4h + 700°C / 24h age, see Figure 3.21 vs. Figures 3.16 through 3.20. In addition, the matrix precipitation for process two using the direct age treatment is finer and of a higher volume fraction than that seen for

process one using the solution + age treatments. The effect of a solution treatment following the forging on the microstructure of alloy 3 is shown in Figure 3.22. There was no noticeable effect of the solution treatment on the carbide morphology.

Voids were observed around some of the carbide reinforcements in the higher carbon, process two alloys, see arrows in Figure 3.21. These voids are believed to be caused by the incomplete flow of the matrix around the carbides or fracture of the carbides during forging. In order to determine the effect of the voids on mechanical strength, a set of specimens from alloy 3 were HIPped at (1250°C / 4 hr). The HIPped properties will be compared later in this report to the unHIPped material to determine strength and ductility differences.

Figure 3.23 illustrates the test specimen geometry for the tensile and creep tests which were performed utilizing ASTM specification E8 and E21. The tensile test temperatures investigated were 21°C (70°F), 538°C (1000°F), & 649°C (1200°F) and creep conditions were 649°C / 175MPa. The alloys 1, 3 & 5 were tested in a range of microstructural conditions. They represent a range of carbide volume fractions from 0 to 16%. No appreciable problem was observed in the machining of these alloys, however it should be noted they were low stress ground at removal rates utilized for less ductile titanium aluminides. This removal rate being approximately half that of conventional Ti alloys. The results of the tensile and creep testing are shown in Tables 3.5 and 3.6. There was only one test performed for each alloy at each temperature. Therefore, the data must be considered preliminary and not conclusive.

It appears that for both process routes the the strength of an alloy increases with increasing volume fraction of carbide phase. Figure 3.24 shows a comparison of the yield strength for alloys 1, 3, and 5 following process one in the as-solution treated and solution and age conditions. The elongation appears to decrease with increasing volume fraction of carbide phase, Figure 3.25, although there is more scatter in the elongation data. All of the elongations measured, with the exception of the 538°C (1000°F) alloy 5 test in the solution and age condition, were above 5% and all of the material conditions appeared ductile. The one test with low ductility had a carbon inclusion on the fracture surface which may have caused the low ductility. As mentioned previously incomplete carbon dissolution in alloy 5 pancakes was observed.

There does not appear to have been any improvement from a direct age following process two compared to a solution and age following process one, Figure 3.26. It was expected that the direct age would have higher strength than the solution and age based on the microstructure observed in the heat treat study. The failed test specimens should be examined to determine whether the correct microstructure was obtained.

The effect of HIP on alloy 3 appears to be a small increase in the ductility at room temperature and strength at all temperatures, Figure 3.27.

The creep data, i.e. time to rupture and final % deformation, indicated that increasing volume fraction of carbide increased the creep resistance of the materials. Also, a solution

and aged structure was more creep resistant than an as-solution treated structure. The direct aged structure does appear to have given an improvement in creep resistance. Finally, HIPing a material gave an improvement in creep resistance compared to an unHIPed structure.

Because of the lack of examination of the test specimens several questions are left open. The failure mechanism, whether the carbide fractures first or the interface between the carbide and matrix fails, is not known. Also whether the actual microstructures were achieved in each of the specimens is not determined. Finally, the large increase in strength for some specimens, such as alloy 5 solution and aged following process 1, was not expected and no explanation can be given.

Wear and Erosion

Erosion testing was accomplished by impinging grit of a specified morphology on the specimen. The angle of incidence, the angle between the specimen surface and the grit trajectory, was either 20° or 90°. The temperature was 21°C (75°F), the grit speed was 200m/s and the grit was classified as runway sand. All three alloys, 1, 3 and 5 were tested in the solution treated and aged condition following process one. Alloy 3 was also tested in the as-solution treated condition (specimen 3B in the figure) for comparison purposes. All three alloys appear to behave as ductile materials in erosion testing. This is based on their higher erosion rates at 20° incidence angle as compared to 90°, Figure 3.28 and 3.29. The low angle of incidence showed virtually no difference between carbide content or heat treatment in regards to erosion resistance. All of these alloys showed similar erosion at 20 degrees to Ti-6Al-4V. At the high angle of impingement several differences were noted. Alloy 3 in the solution treated and aged condition showed improvement in erosion resistance over the solution treated version. All of the new alloys, including alloy 1 which had no carbide, had about a 2X improvement in erosion resistance over Ti-6Al-4V at 90°. There does not appear to have been any effect of the carbide phase on the erosion resistance compared to the base alloy which contained no carbide.

The sliding wear test was performed at 175°C (350°F) with a stress of 372MPa, and a frequency of 60CPM. Sliding wear resistance for the new alloys was generally poor compared to Ti-6Al-4V, Table 3.7. Alloy 1 showed massive plastic deformation and galling which resulted in higher friction coefficients and dimensional material losses. Alloy 5, with the higher carbide content had better wear resistance, although the yielding and adhesive material transfer were still present. Friction coefficients were also reduced for alloy 5. The best results were obtained with Ti-6Al-4V. Very low amounts of wear were seen and friction coefficients were slightly lower than for alloy 5. Very little galling was noted.

A more significant analysis of the surfaces and property differences between the three alloys would be required to determine probable causes of these unexpected results. It does appear from the limited wear testing performed that the carbide phase does improve the wear resistance of the base alloy.

3.0 Summary and Conclusions

Ingots of the required composition were produced with minimal difficulties. Some carbon inclusions were found in the highest carbon containing alloys, however it is believed that with alternate methods of adding carbon to the melt the inclusions could be eliminated. The morphology of the carbide phase can be manipulated through thermomechanical processing of the cast material. The process route chosen does have an effect on the microstructure parameters of the carbide phase. The carbide phase that forms is based on the structure Ti_2C with Nb substituting for some of the Ti.

The strength of the alloy increases and the ductility decreases with increasing carbon content. Some of the alloys exhibited very high strengths at room temperature. The wear and erosion results were less than expected. The erosion resistance was better than Ti-6Al-4V at 90° incidence but about the same at 20° incidence. The wear was poorer than Ti-6Al-4V.

4.0 Future Recommendations

The unexpected results identified in this study should be investigated. Specifically the very high strengths obtained for some of the conditions are suspect, especially since only one test was performed. The unexpected wear and erosion results should also be investigated. The test specimens should be analyzed to determine that the expected microstructure was obtained. The tradeoffs among wear and erosion resistance, strength and ductility should be quantified. Larger scale ingots of selected compositions should be produced and reduced to billet to demonstrate metalworking practices for these materials. Concurrently, alternate base alloys should be investigated to improve the matrix properties.

5.0 References

1) Karen D. Jones, M.S. Thesis, Rensselaer Polytechnic Institute, 1990

2) D.G. Konitzer & M.H. Loretto, "Microstructural Assessment of Ti6Al4V-TiC MMC", Acta Metall., Vol. 37, No.2, pp.397-406, 1989.

3) D.G. Konitzer etal, Final Report of contract F33615-87-C-5298, "Rapidly Solidified Oxidation Resistant Niobium Base Alloys", 1993

4) D.G. Konitzer, GE IR&D, 1992

Table 3.1; Composition in atomic percent and density of screening alloys

Composition					Measured Density	
Alloy #	Ti	Nb	Al	C	g/cc	Pounds / in^3
1	50.5	40.5	9	0	6.095	0.220
2	49.8	40	8.9	1.3		
3	49.2	39.5	8.8	2.5	6.093	0.220
4	48	38.5	8.5	5		
5	46.7	37.5	8.3	7.5	6.062	0.219

Table 3.2; Composition of screening alloys in weight percent

Alloy #	Ti	Nb	Al	C
1	37.6	58.6	3.8	0
2	37.5	58.5	3.8	0.2
3	37.4	58.3	3.8	0.5
4	37.3	58	3.7	1
5	37.1	57.7	3.7	1.5

Table 3.3; Microprobe analysis on solution treated alloy phases (atomic %)

Alloy #	S.T.	Phase	Ti	Nb	Al	C(*)
1	1050°C/24 h	Carbide	75.80	12.56	0.91	10.73
1	1050°C/24 h	Matrix	36.10	60.09	3.44	00.38
2	1050°C/24 h	Carbide	74.66	14.31	0.08	10.96(+)
2	1050°C/24 h	Matrix	36.26	62.31	0.37	01.07(+)
3	1050°C/24 h	Carbide	67.45	20.94	0.66	10.95
3	1050°C/24 h	Matrix	36.09	59.75	4.15	00.00
4	1050°C/24 h	Carbide	60.32	29.32	0.53	09.83
4	1050°C/24 h	Matrix	33.89	62.31	3.80	00.00
5	1050°C/24 h	Carbide	53.63	35.89	0.33	10.16
5	1050°C/24 h	Matrix	32.99	62.02	4.12	00.88
3	1200°C/24 h	Carbide	71.66	16.76	0.51	11.07
3	1200°C/24 h	Matrix	35.33	60.69	3.99	00.00
3	1350°C/4 h	Carbide	69.55	17.56	0.32	12.57
3	1350°C/4 h	Matrix	36.43	59.57	4.00	00.00

() - Formula utilized 100-%(Ti+Nb+Al) = %C;*
(+) - Alloy 2 had low Al in melt.

Table 3.4. Thermal Treatments Studied for Both Processes

CONDITION	PROCESS 1	PROCESS 2
Forge+Solution (1350°C / 4 hr)	√	
Forge+Solution(1350°C / 4 hr)+Age	√	
Solution(1350°C / 4 hr)+Forge		√
Solution+Forge+Direct Age(700°C / 24 hr)		√
Solution+Forge+Solution/Anneal(1250°C / 4 hr)		√
Solution+Forge+Solution+Age		√

Table 3.5; Tensile test results

Spec.	*Alloy*	*Condition*	*Test Temp.*		*0.2% Y.S.*		*UTS*		*Elongation*	*R. of A.*
			°F	*°C*	*Ksi*	*MPa*	*Ksi*	*MPa*	*%*	*%*
		Forge+1350°C/4h								
1AS	1	As-Solution	70	21	67.1	462.7	70.3	484.7	17.1	68
1AS	1	As-Solution	1000	538	33.8	233.1	34.4	237.2	29.4	75.5
1AS	1	As-Solution	1200	649	34.7	239.3	35	241.3	18.3	17.9
3AS	3	As-Solution	70	21	84.2	580.6	89.6	617.8	8.8	17.9
3AS	3	As-Solution	1000	538	55.2	380.6	66.7	459.9	15.8	29.9
3AS	3	As-Solution	1200	649	52.3	360.6	57.4	395.8	26.1	47.9
5AS	5	As-Solution	70	21	79.8	550.2	99.8	688.1	5.9	15.6
5AS	5	As-Solution	1000	538	65.4	450.9	79.3	546.8	8.2	19.7
5AS	5	As-Solution	1200	649	69	475.8	75.1	517.8	7.3	19.9
1ASA	1	700°C/50h Age	70	21	159.9	1102.5	159.9	1102.5	11.8	34
1ASA	1	700°C/50h Age	1000	538	42.8	295.1	44.1	304.1	16.6	67.7
1ASA	1	700°C/50h Age	1200	649	37.9	261.3	39.4	271.7	16	62.5
3ASA	3	700°C/50h Age	70	21	170.2	1173.5	188.8	1301.8	16.3	32.1
3ASA	3	700°C/50h Age	1000	538	54.3	374.4	67.1	462.7	17.3	42.3
3ASA	3	700°C/50h Age	1200	649	49.9	344.1	58.9	406.1	23.8	54.7
5ASA	5	700°C/50h Age	70	21	194.4	1340.4	217.9	1502.4	8.9	15.7
5ASA	5	700°C/50h Age	1000	538	77.1	531.6	86.5	596.4	2.4	7.7
5ASA	5	700°C/50h Age	1200	649	71.4	492.3	80.4	554.4	9.4	25.5
		1350°C/4h+Forge								
3BS	3	1250°C/4h Sol.	70	21	162.6	121.1	166.2	1145.9	7.7	15.8
3BS	3	1250°C/4h Sol.	1000	538	46.9	323.4	58.7	404.7	17.9	40.3
3BS	3	1250°C/4h Sol.	1200	649	44	303.4	48.1	331.6	17.5	46.2
3BSA	3	Solution+Age	70	21	No test, extensometer failure					
3BSA	3	Solution+Age	1000	538	67.1	462.7	84.3	581.2	8.9	24.3
3BSA	3	Solution+Age	1200	649	52.3	360.6	64.2	442.7	17.2	43.8
3BDA	3	700°C/24h DA	70	21	81.8	564.0	89.5	617.1	6.1	13.9
3BDA	3	700°C/24h DA	1000	538	56.1	386.8	67	462.0	8.9	20.5
3BDA	3	700°C/24h DA	1200	649	55.4	382.0	58	399.9	13.9	29.2
5BDA	5	700°C/24h DA	70	21	103.2	711.6	109.2	752.9	1.5	3.4
5BDA	5	700°C/24h DA	1000	538	82.6	569.5	87.5	603.3	2.2	4.5
5BDA	5	700°C/24h DA	1200	649	69.6	479.9	77.7	535.7	5.1	10.1
3BH	3	HIP(Solution)	70	21	169.9	1171.5	173.8	1198.4	14.9	20.2
3BH	3	HIP(Solution)	1000	538	54.3	374.4	65.9	454.4	18.1	34.9
3BH	3	HIP(Solution)	1200	649	49.3	339.9	53.1	366.1	21.5	48.1

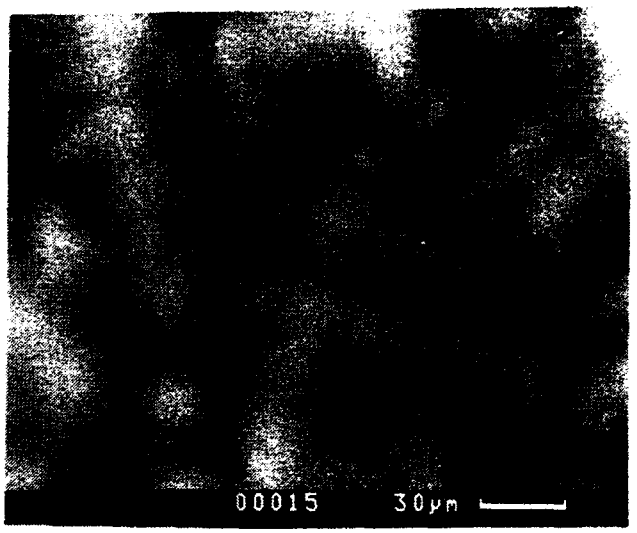
Table 3.6; Creep test results

Spec.	*Alloy*	*Condition*	*Rupture (h)*	*% Elongation*	*% R of A*	*Final Time (h)*	*Final % Defor.*
		Forge+1350°C/4h					
1AS	1	As-Solution	5.8	28.4	74.5	5.4	6.456
3AS	3	As-Solution	17.1	21.4	21.7	15.7	20.544
5AS	5	As-Solution	100*			100	2.29
1ASA	1	700°C/50h Age	4.1	29.6	53.4	2.5	3.494
3ASA	3	700°C/50h Age	100*			100	4.687
5ASA	5	700°C/50h Age	100*			100	1.467
		1350°C/4h+Forge					
3BS	3	1250°C/4h Sol.	12.8	24	30.7	12.5	15.245
3BH	3	HIP(Solution)	100*			100	1.839
3BDA	3	700°C/24h DA	100*			100	1.608
5BDA	5	700°C/24h DA	100*			100	1.33
3BSA	3	Solution+Age	100*			100	2.59

* Test stopped

Table 3.7; Wear test results for testing at 175C, 370MPa, and 10,000 strokes

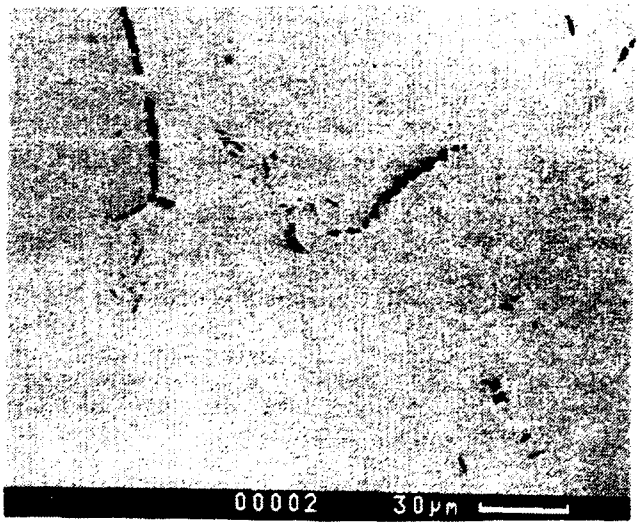
Alloy	*Test*	*Stroke (mm)*	*Material Wear (mm)* *Block*	*Shoe*	*Friction* *Initial*	*Final*
1	1	0.013	-0.076	-0.018	0.86	0.81
1	2	0.013	-0.132	-0.048	0.89	0.88
5	1	.008-.023	-0.076	0.033	0.8	0.56
5	2	.008-.018	-0.02	-0.003	0.46	0.65
Ti-6Al-4V	1	.008-.015	-0.01	-0.005	0.46	0.57



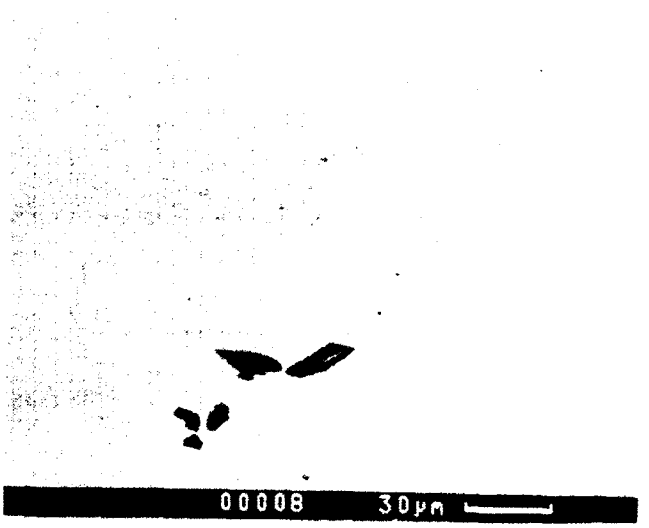
a



b

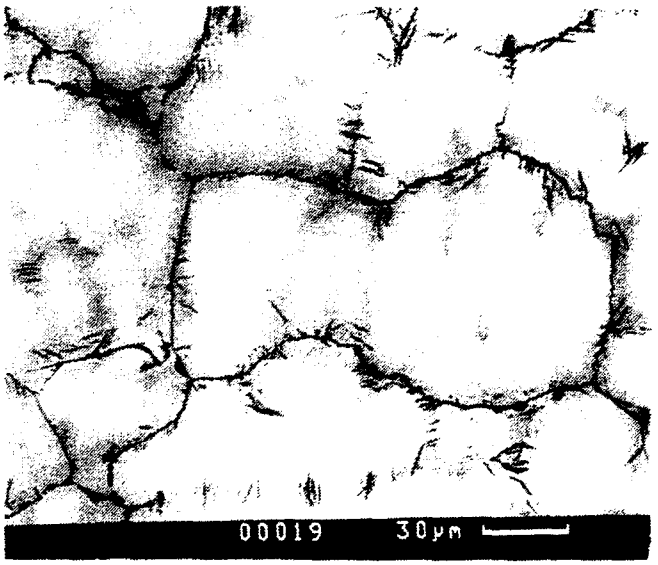


c

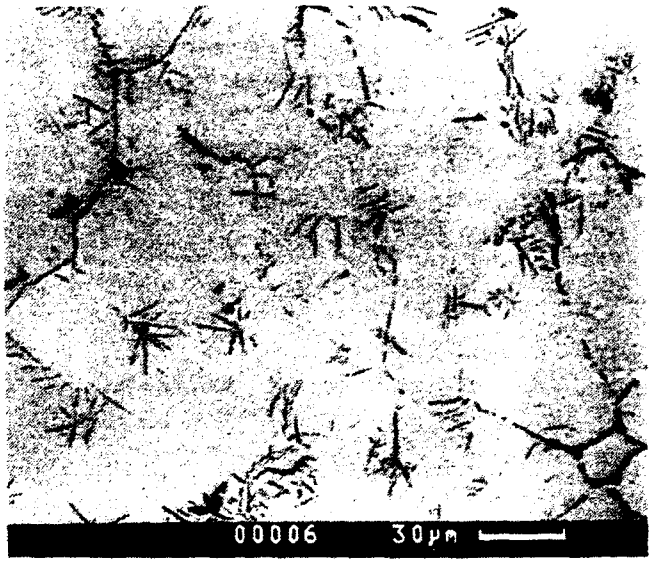


d

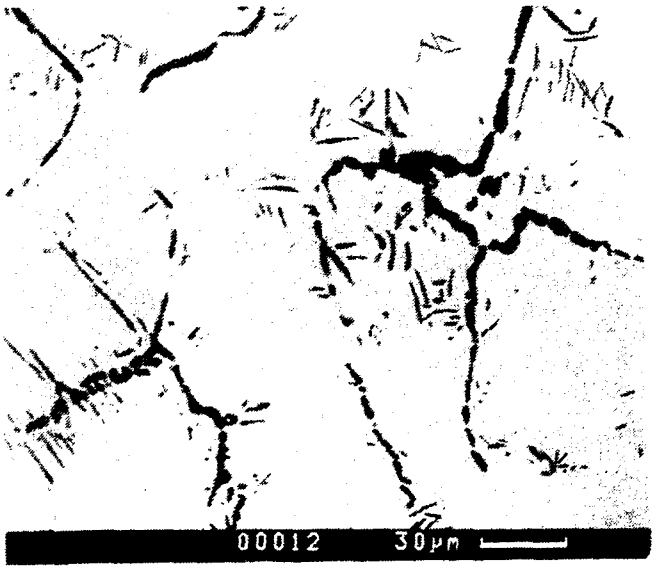
Figure 3.1; Backscattered electron micrographs of specimens of composition 50.5Ti-40.5Nb-9Al in the a) as-cast and heat treated at b) 1050C / 24h, c) 1200C / 24h, and d) 1350C / 4h.



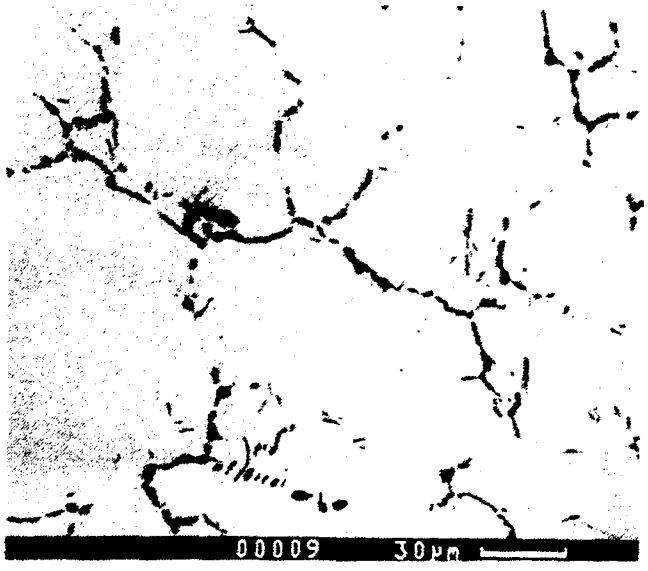
a



b



c



d

Figure 3.2; Backscattered electron micrographs of specimens of composition 49.8Ti-40Nb-8.9Al-1.3C in the a) as-cast and heat treated at b) 1050C / 24h, c) 1200C / 24h, and d) 1350C / 4h.

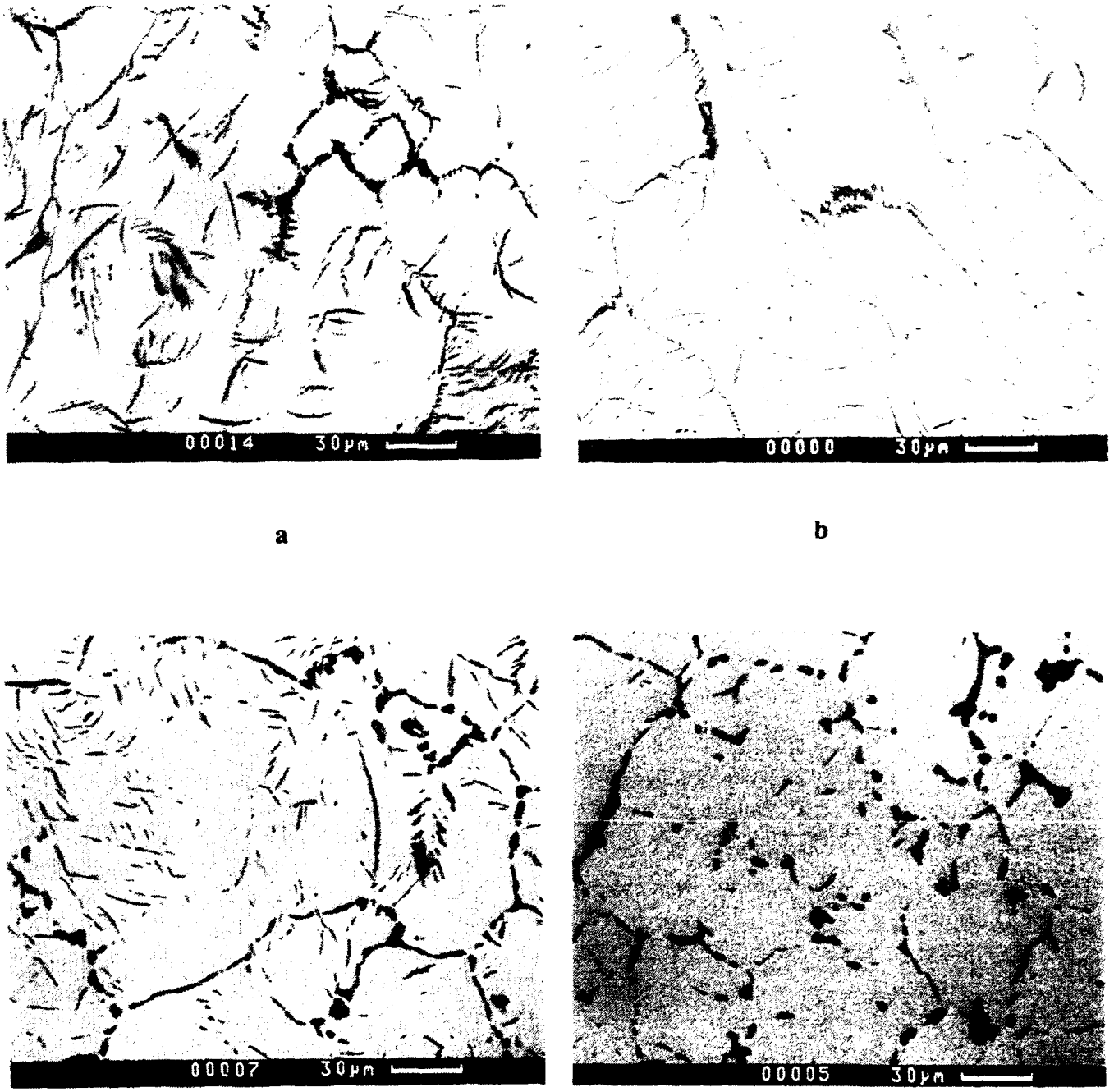
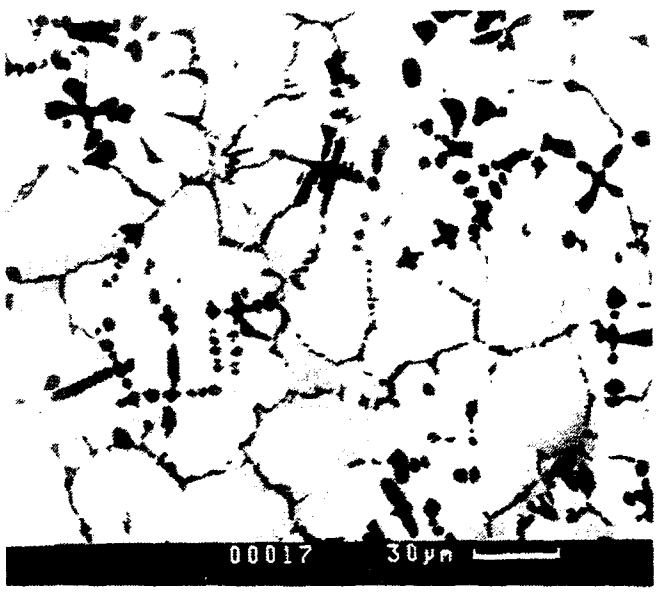
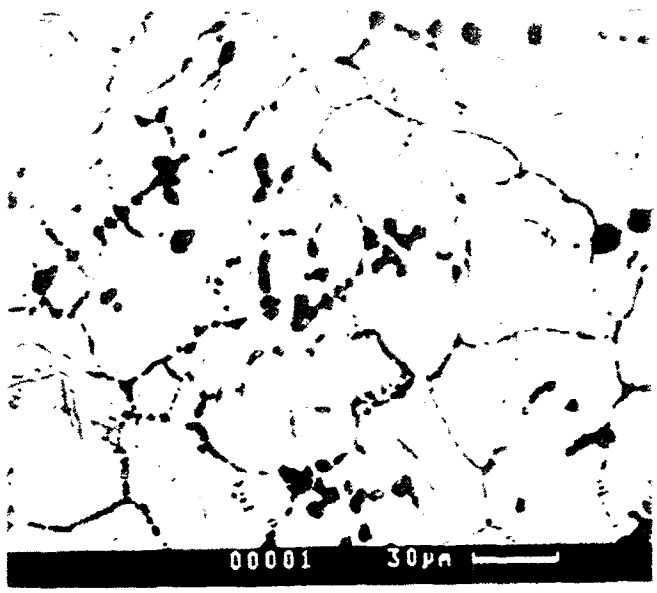


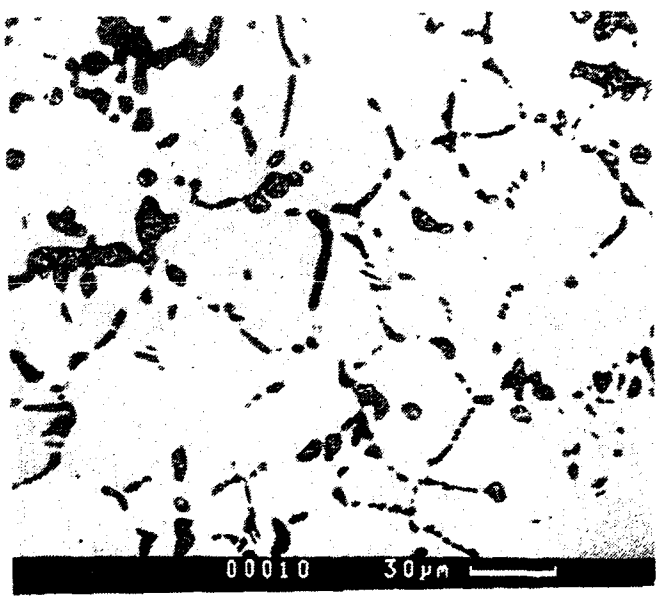
Figure 3.3; Backscattered electron micrographs of specimens of composition 49.2Ti-39.5Nb-8.8Al-2.5C in the a) as-cast and heat treated at b) 1050C / 24h, c) 1200C / 24h, and d) 1350C / 4h.



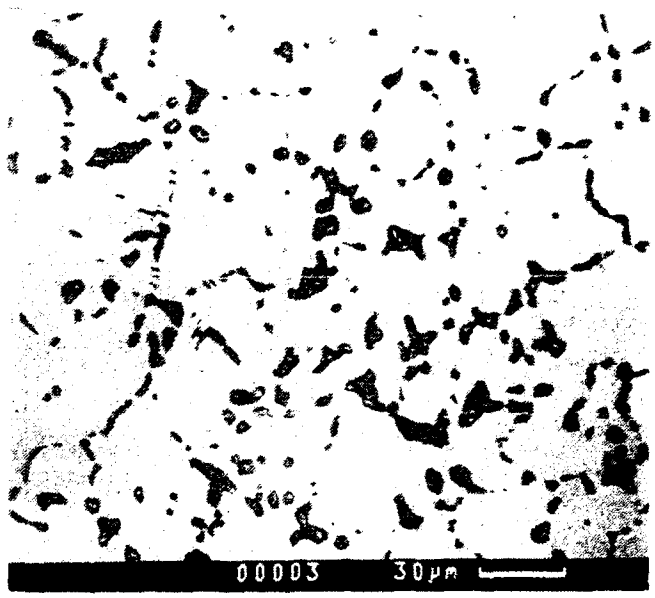
a



b

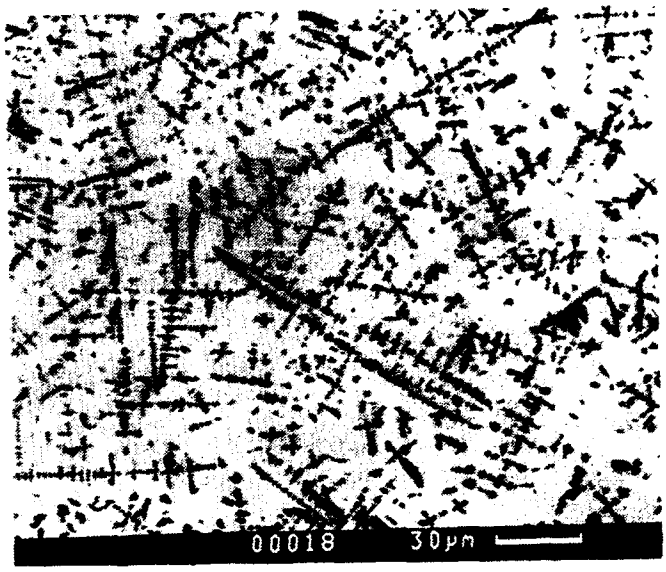


c

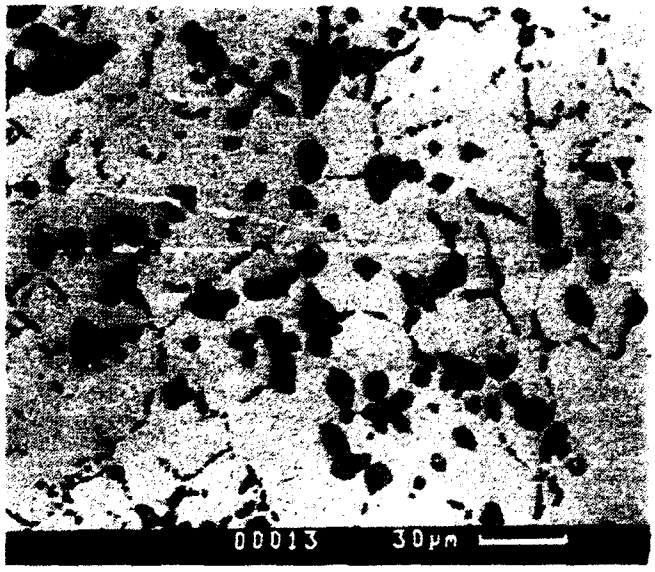


d

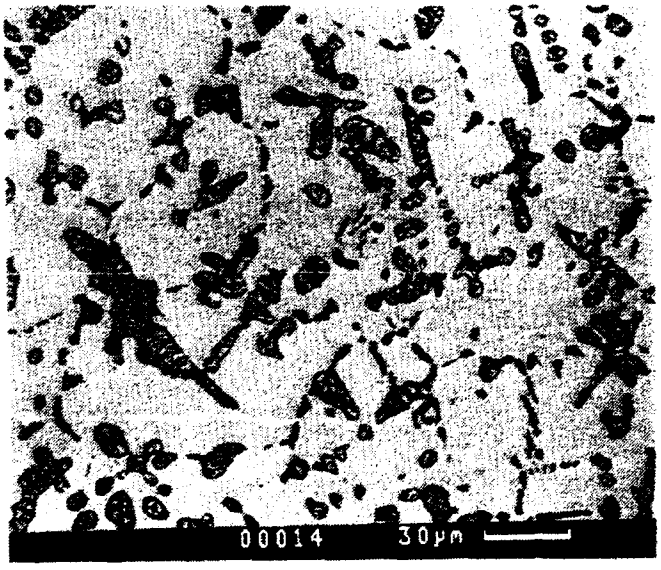
Figure 3.4; Backscattered electron micrographs of specimens of composition 48Ti-38.5Nb-8.5Al-5C in the a) as-cast and heat treated at b) 1050C / 24h, c) 1200C / 24h, and d) 1350C / 4h.



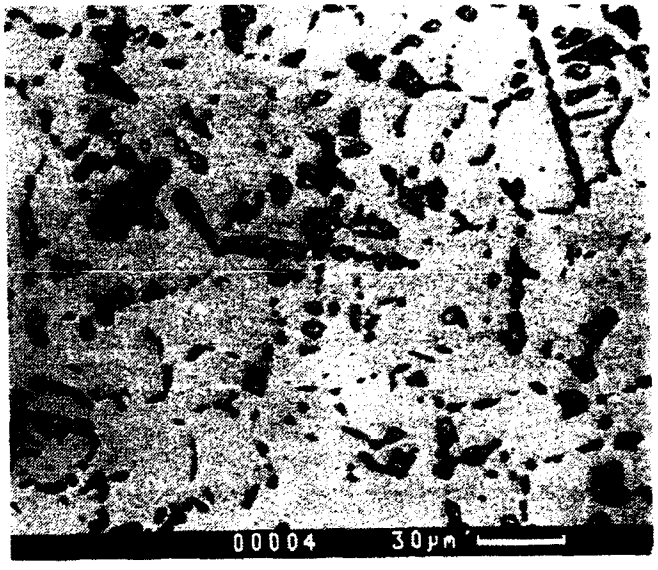
a



b



c



d

Figure 3.5; Backscattered electron micrographs of specimens of composition 46.7Ti-37.5Nb-8.3Al-7.5C in the a) as-cast and heat treated at b) 1050C / 24h, c) 1200C / 24h, and d) 1350C / 4h.

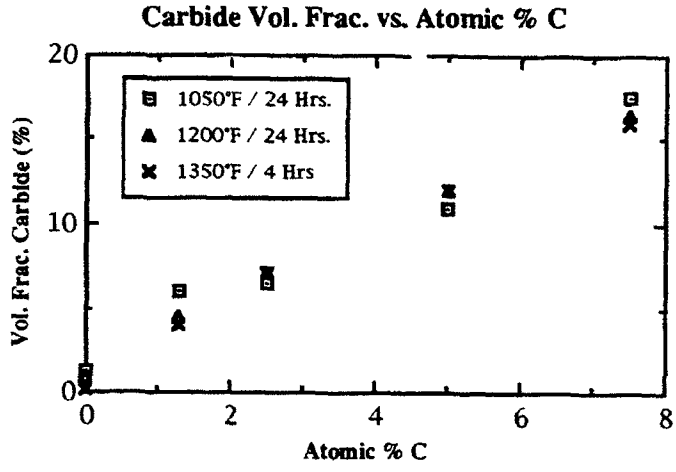


Figure 3.6; Plot of carbide volume fraction vs. carbon content relationship.

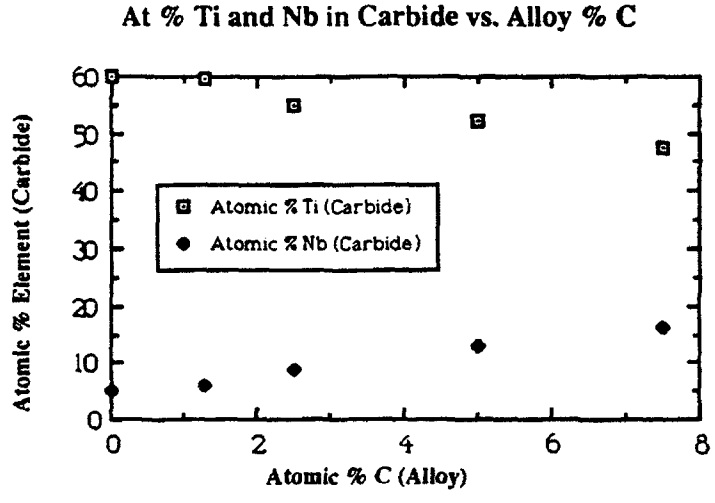


Figure 3.7; Plot of Nb and Ti content in the carbide phase as a function of alloy carbon content.

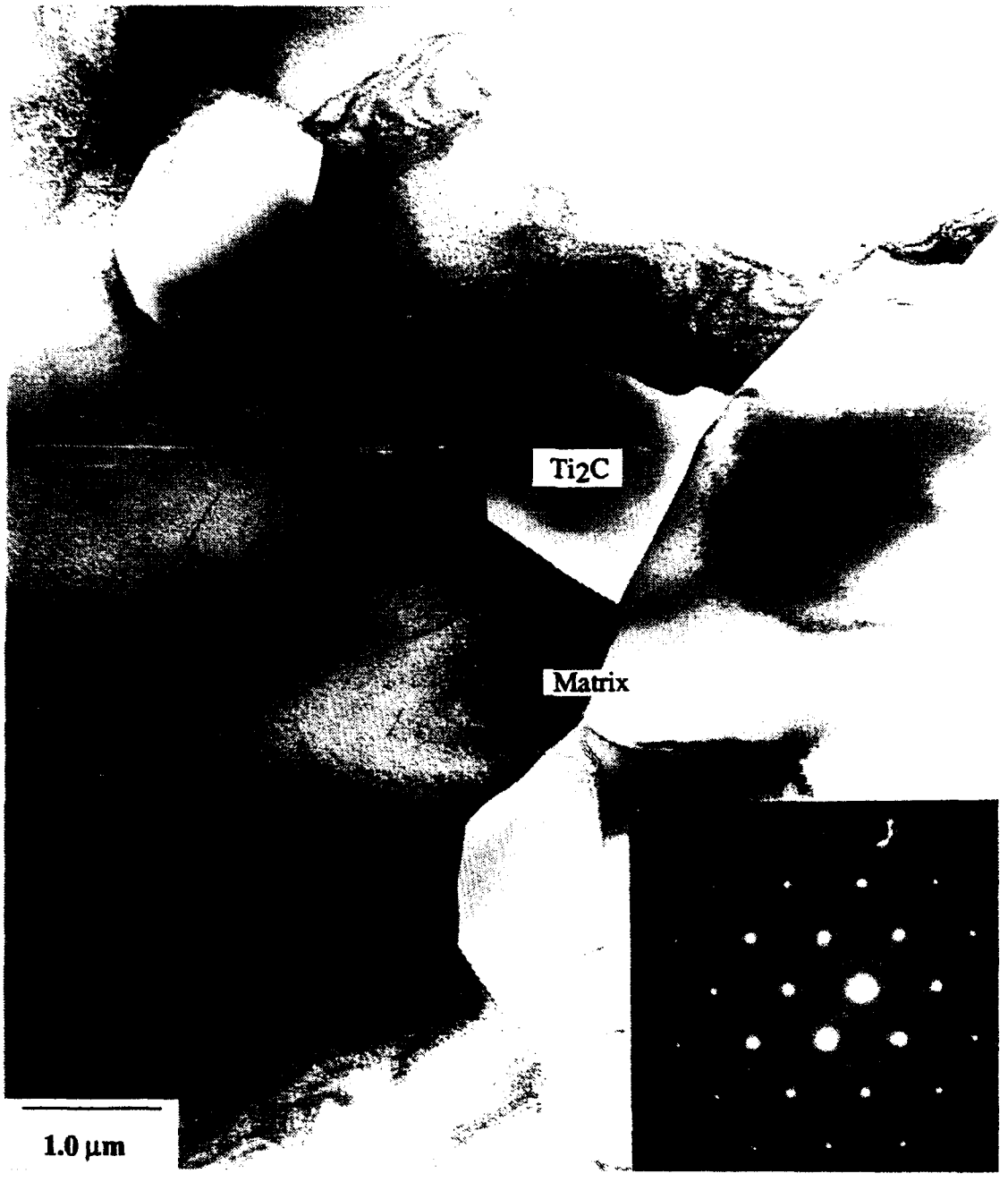


Figure 3.8; Transmission electron microscope bright field images of alloy 5 microstructure with selected area diffraction [101] zone axis pattern indicating the presence of Ti_2C Carbide (Alloy)

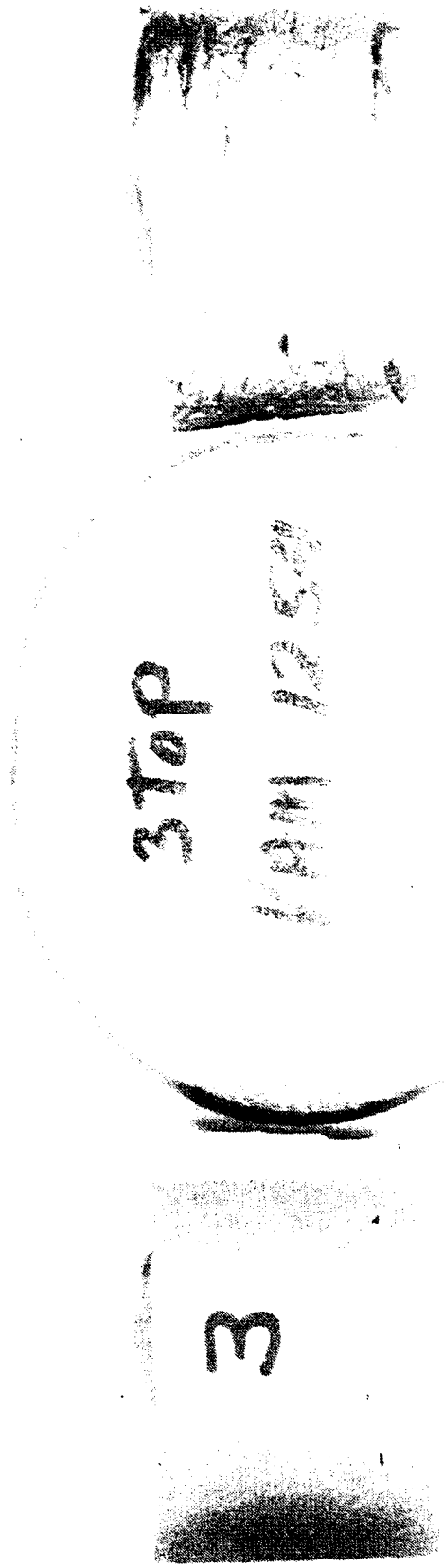


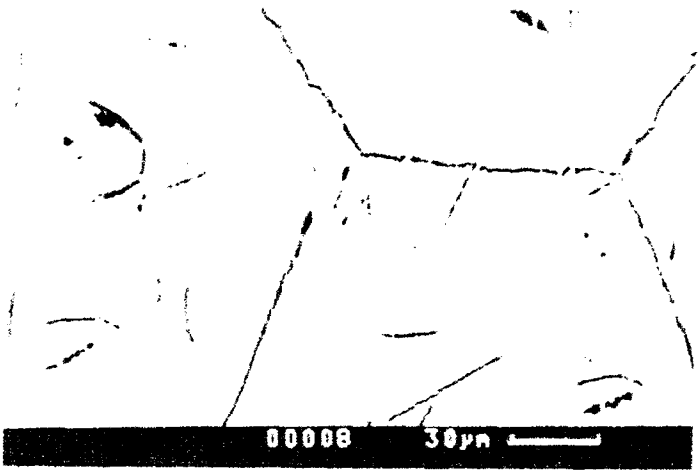
Figure 3.9; Forged pancake and cast ingot shells, magnification 2/3X



Figure 3.10; Texture along pancake edges, magnification 3/4X



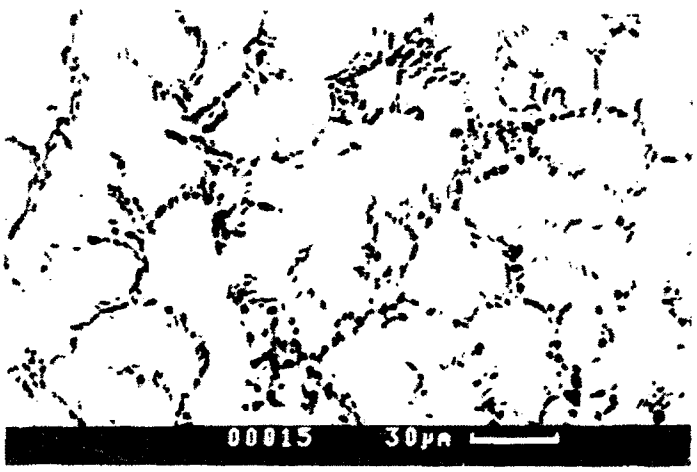
Alloy 1



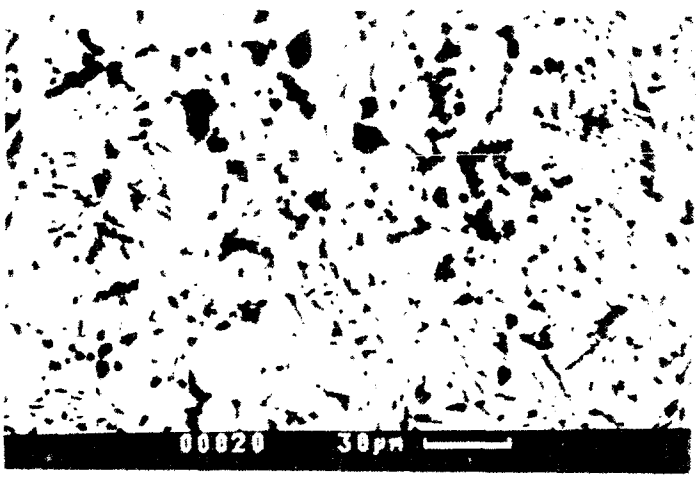
Alloy 2



Alloy 3

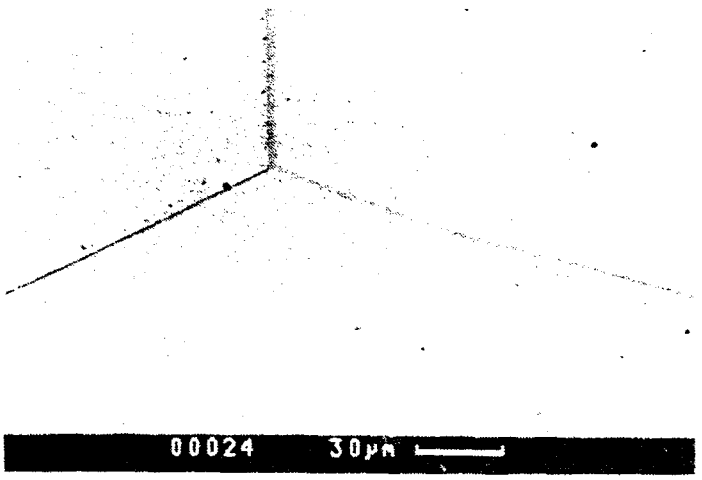


Alloy 4

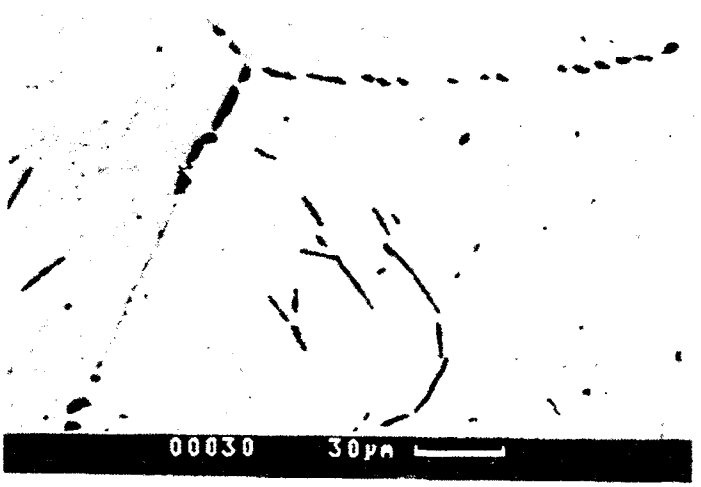


Alloy 5

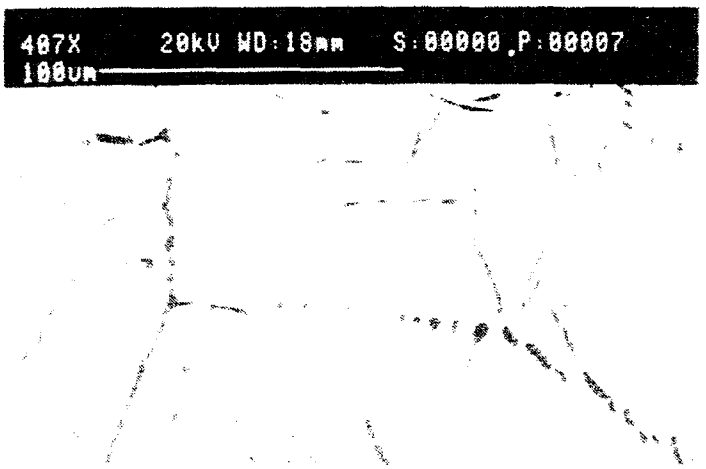
Figure 3.11: Backscattered electron micrographs of the as-cast structure of alloys 1 through 5 showing the carbide phase distributed throughout the beta phase matrix.



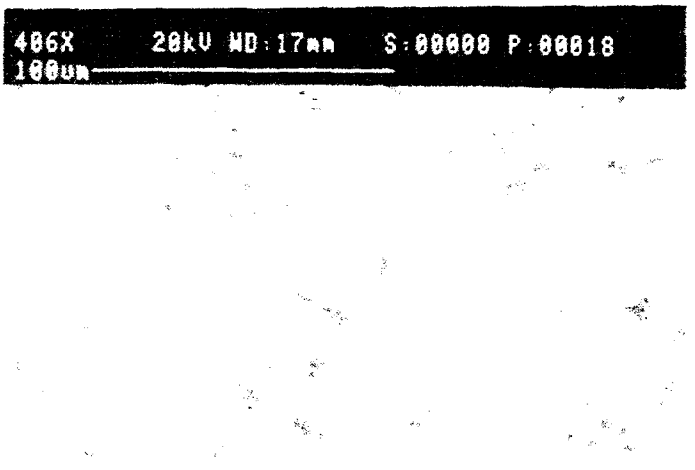
Alloy 1



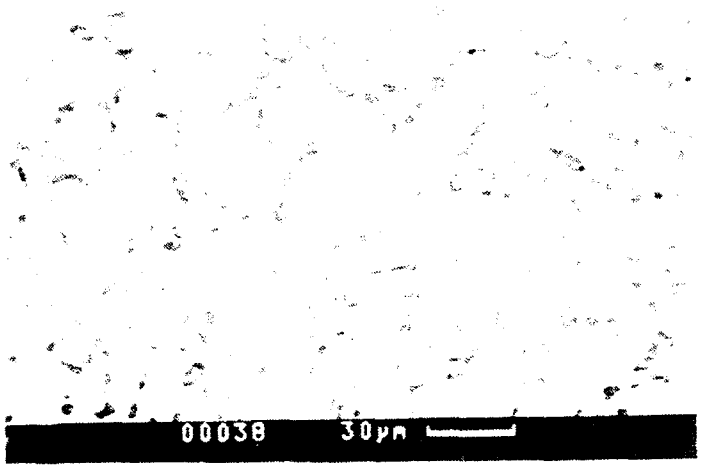
Alloy 2



Alloy 3

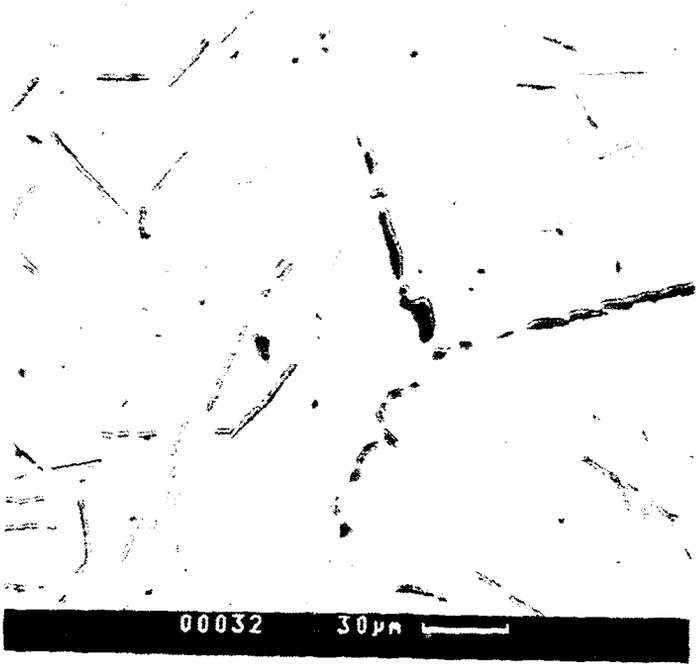


Alloy 4

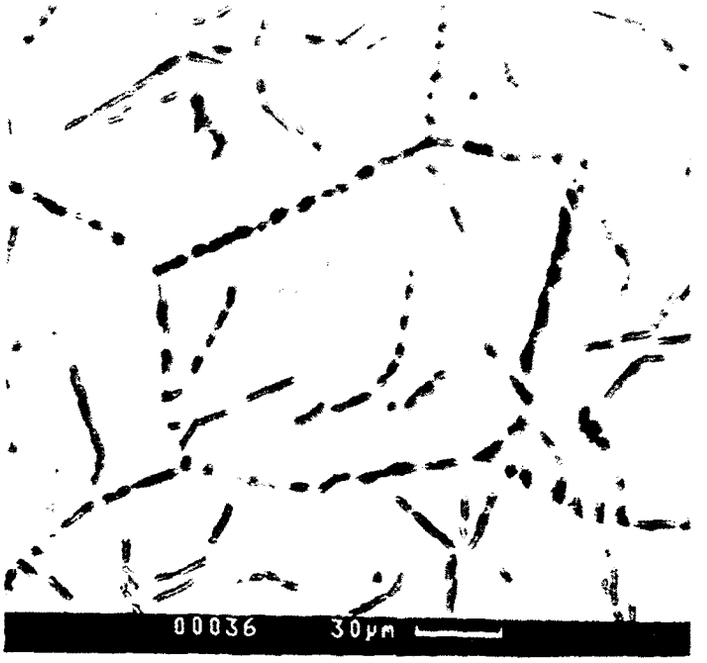


Alloy 5

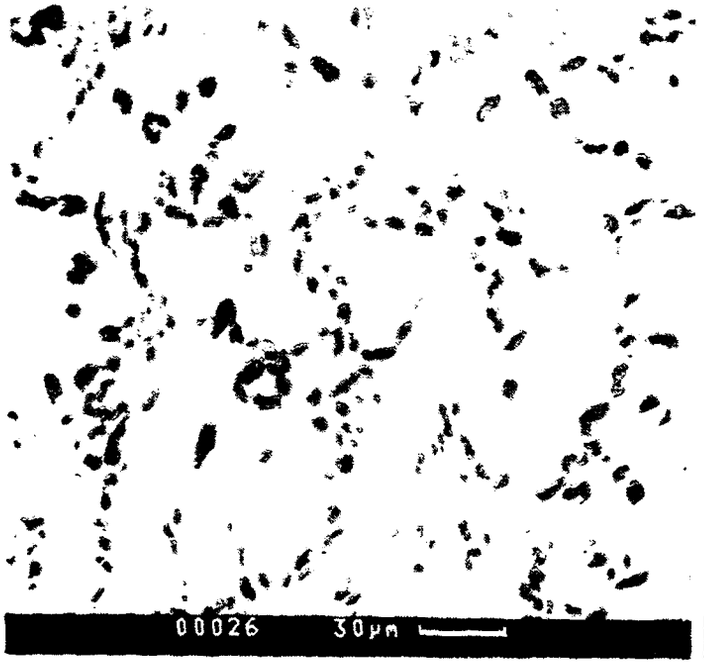
Figure 3.12; Backscattered electron micrographs of alloys 1-5 which were heat treated to simulate the thermal cycles prior to forging for process 1, i.e. 1100C / 0.5h



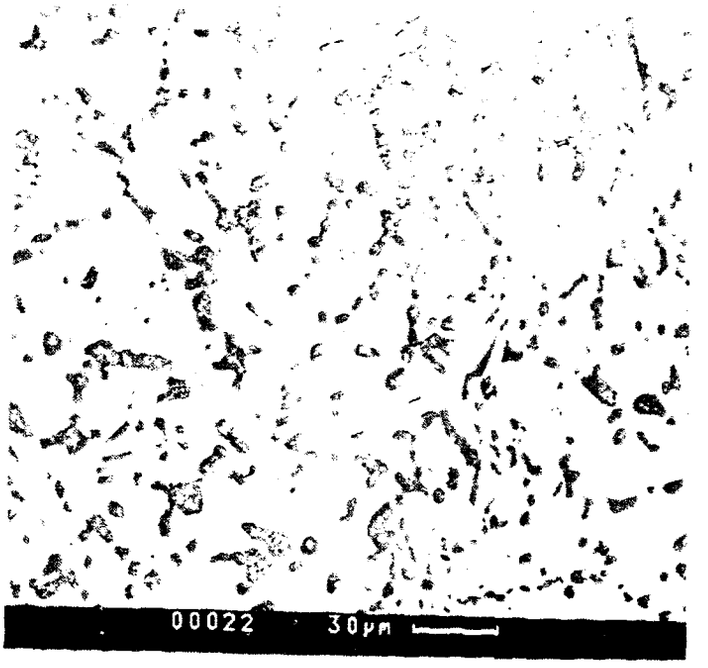
Alloy 2



Alloy 3

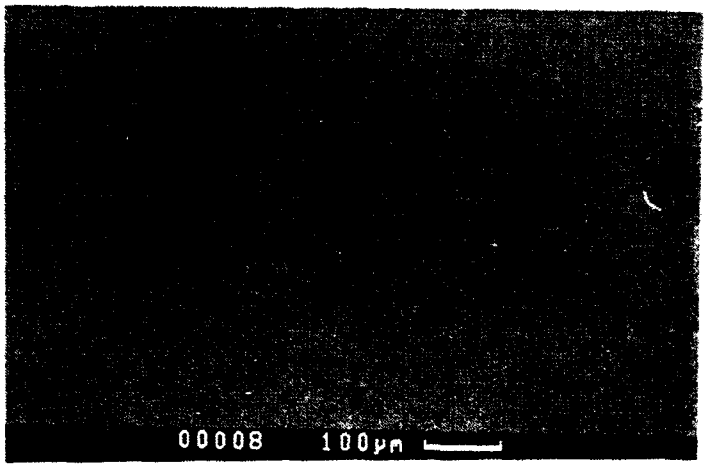


Alloy 4

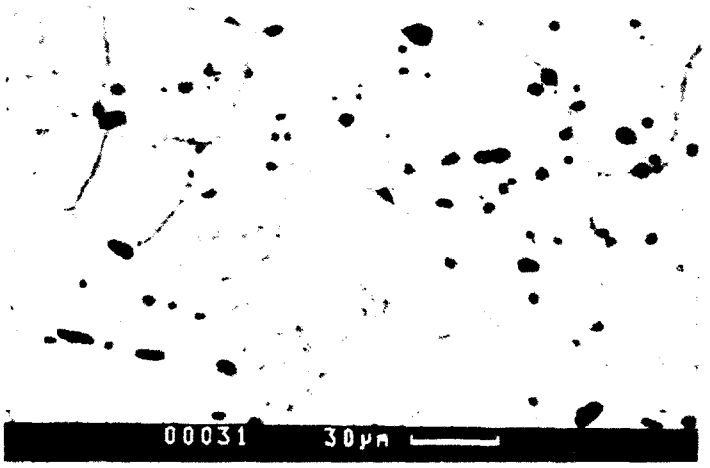


Alloy 5

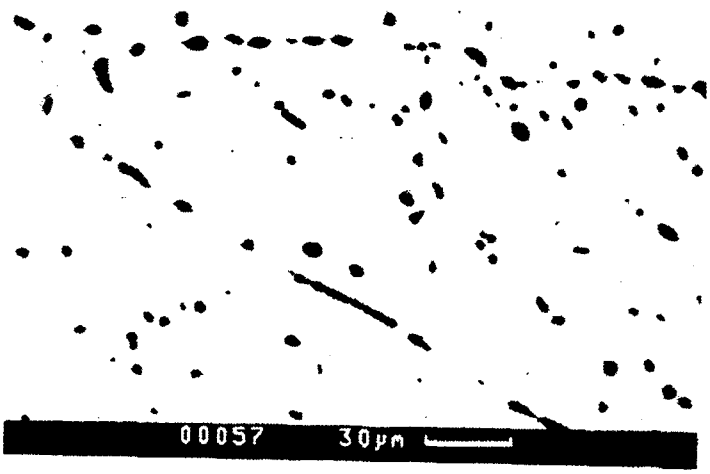
Figure 3.13; Backscattered electron micrographs of alloys 2-5 which were heat treated to simulate the thermal cycles prior to forging for process 2, i.e.1350C / 4h plus 1100C / 0.5h



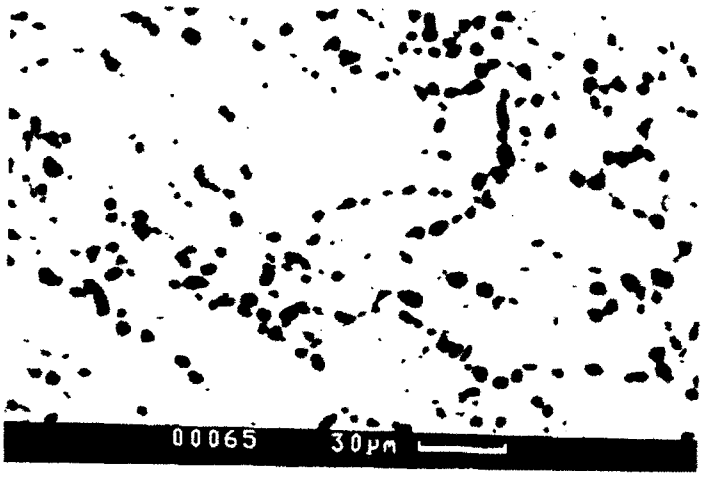
Alloy 1



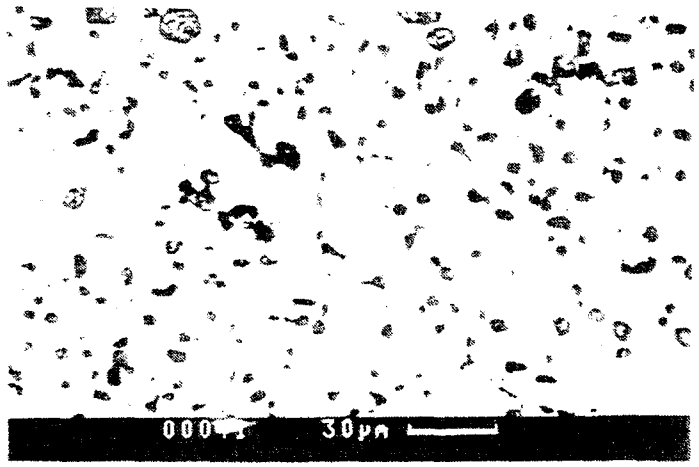
Alloy 2



Alloy 3

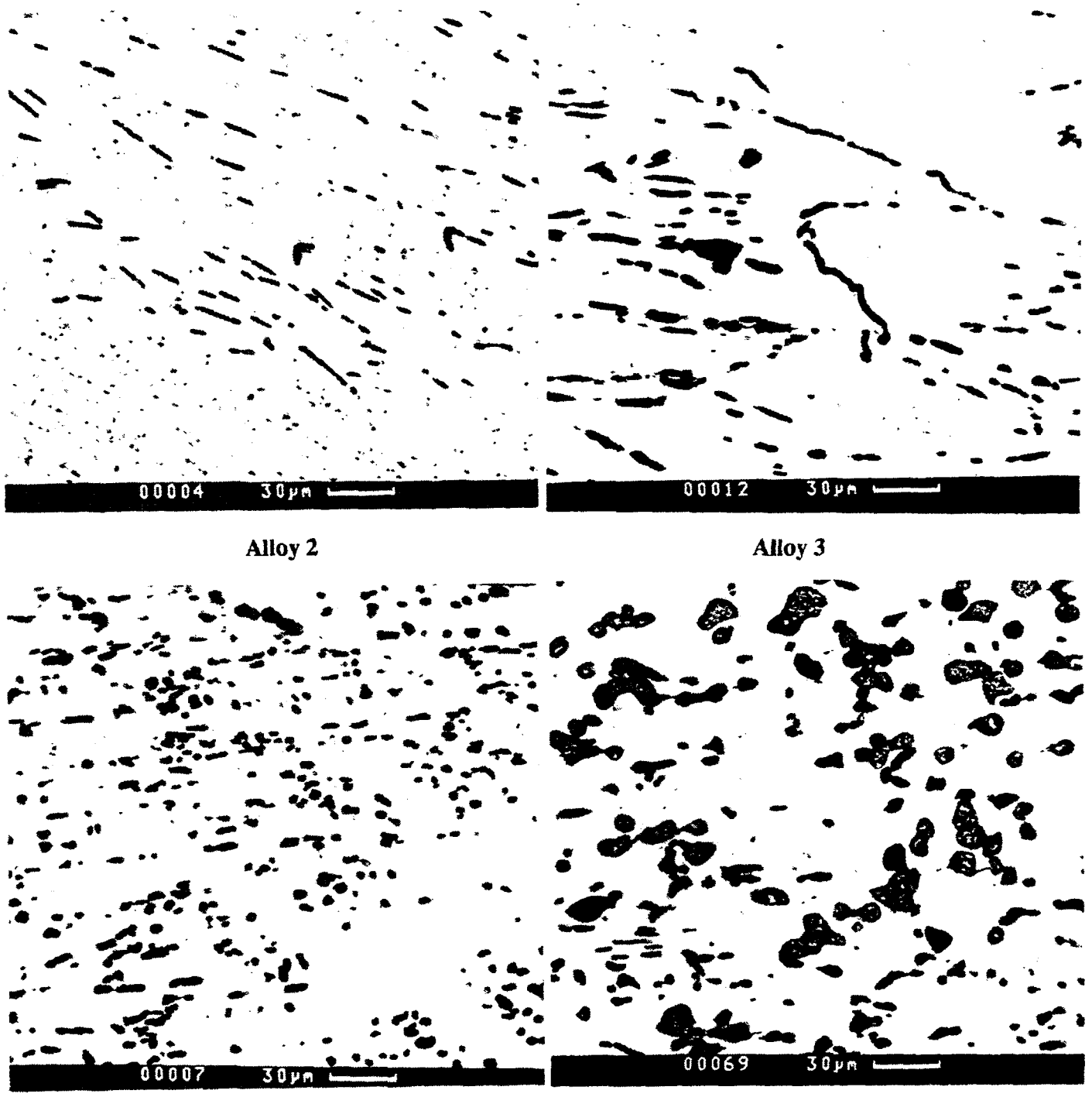


Alloy 4



Alloy 5

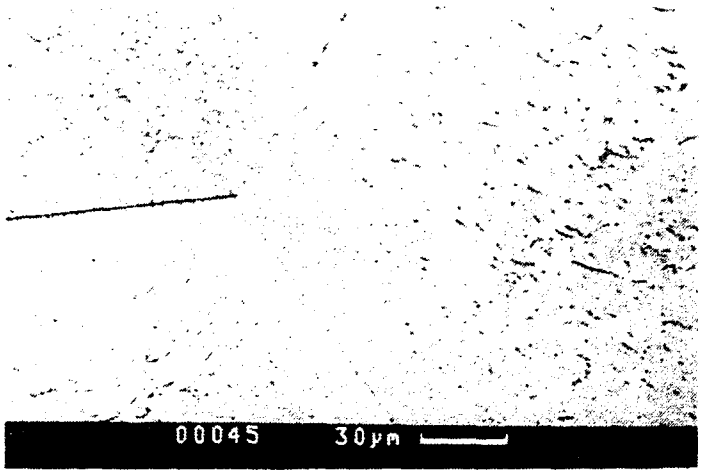
Figure 3.14; Backscattered electron micrographs of alloys 1-5 which were forged plus solution treated at 1350C / 4h, process 1



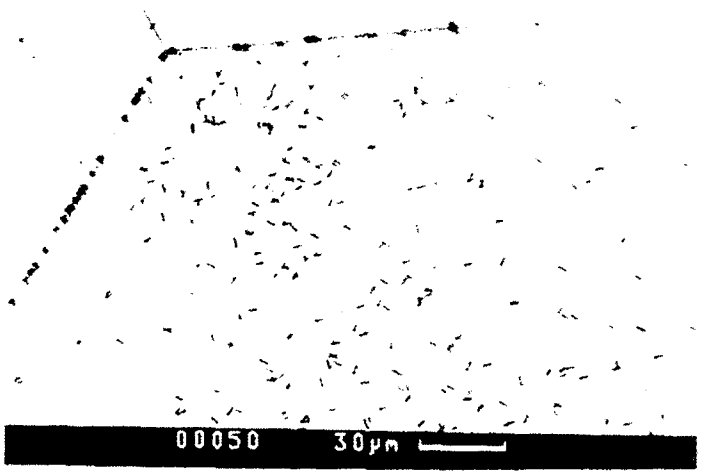
Alloy 2 **Alloy 3**

Alloy 4 **Alloy 5**

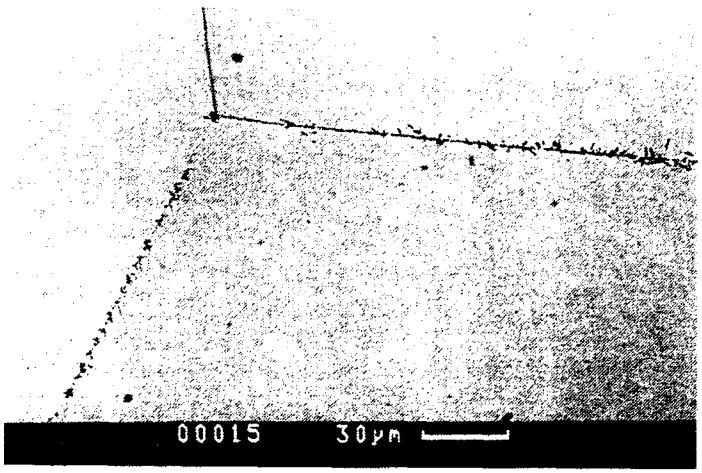
Figure 3.15; Backscattered electron micrographs of alloys 2-5 which were solution treated at 1350°C/4h and subsequently forged, process 2



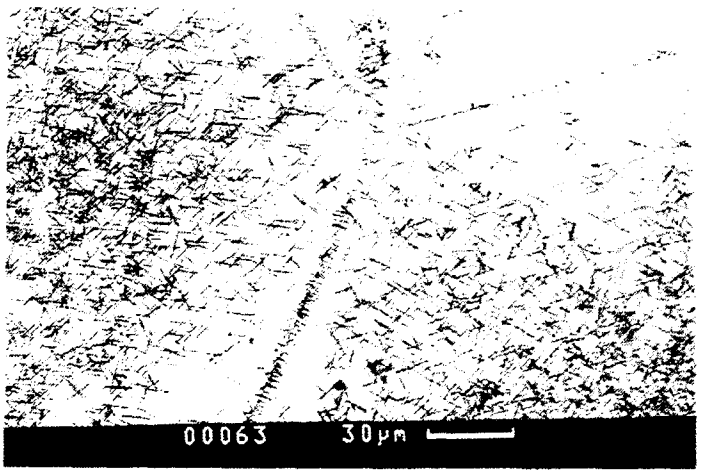
600°C / 24h



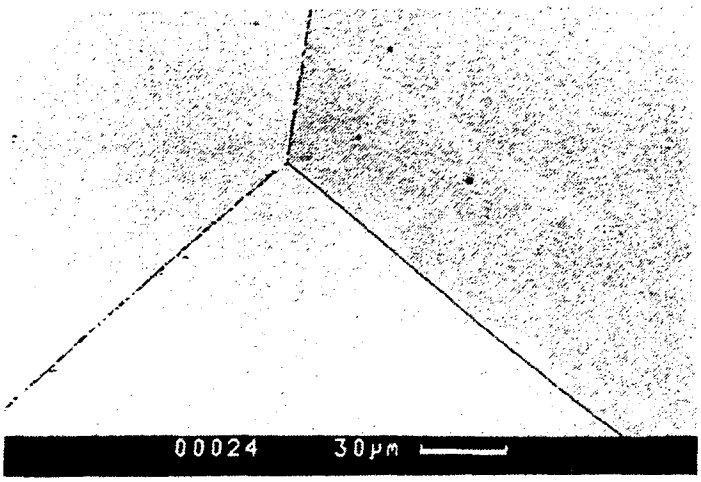
650°C / 24h



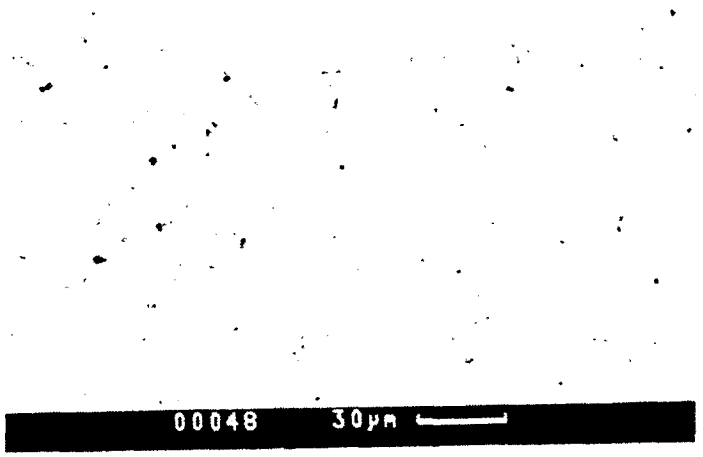
700°C / 24h



700°C / 50h

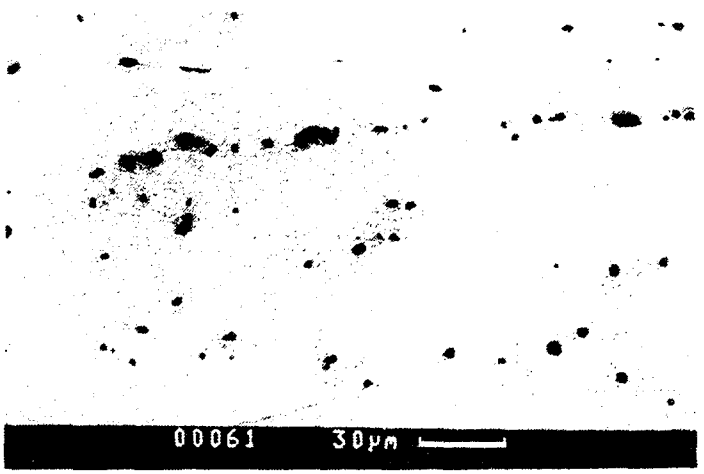


750°C / 24h

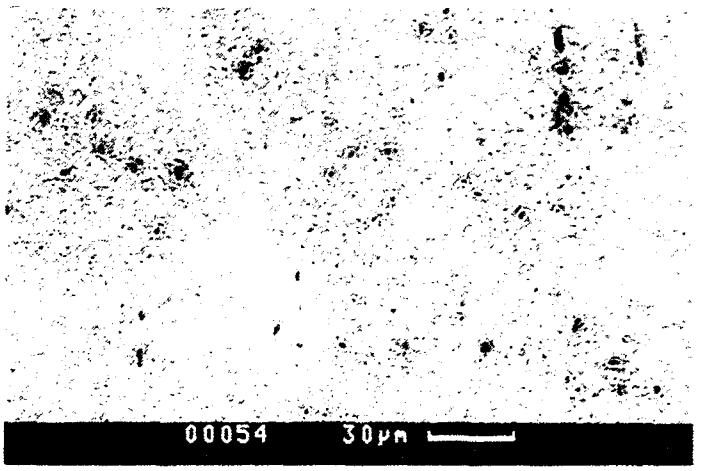


800°C / 24h

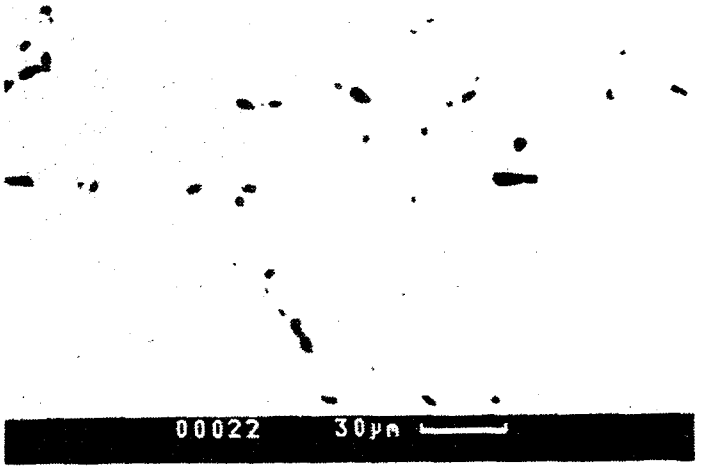
Figure 3.16; Backscattered electron images of microstructures of alloy 1 which was aged for various times and temperatures following process 1, forging plus solution treatment at 1350C / 4h.



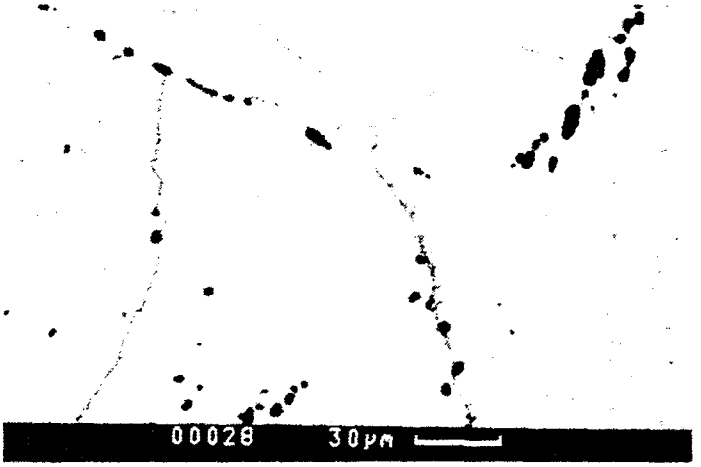
600°C / 24h



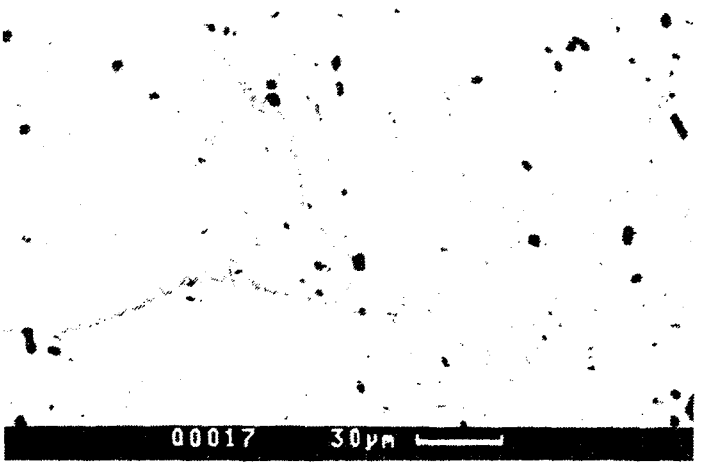
650°C / 24h



700°C / 24h

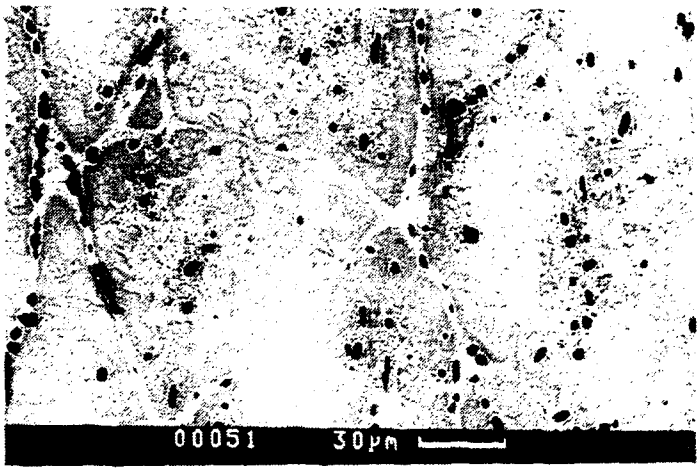


750°C / 24h

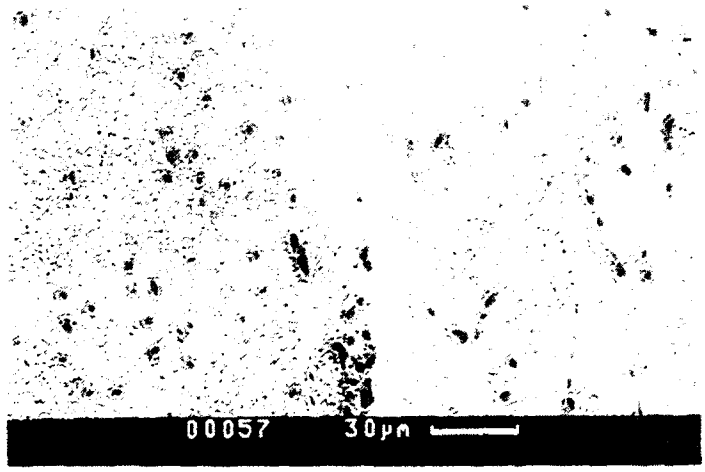


800°C / 24h

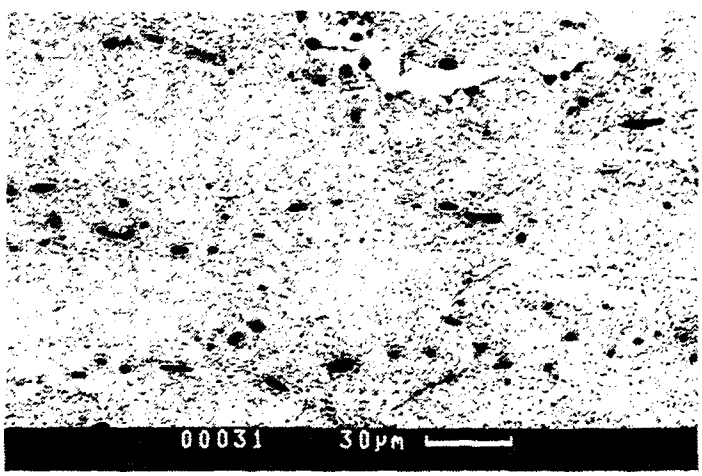
Figure 3.17; Backscattered electron images of microstructures of alloy 2 which was aged for 24h at various temperatures following process 1, forging plus solution treatment at 1350C / 4h.



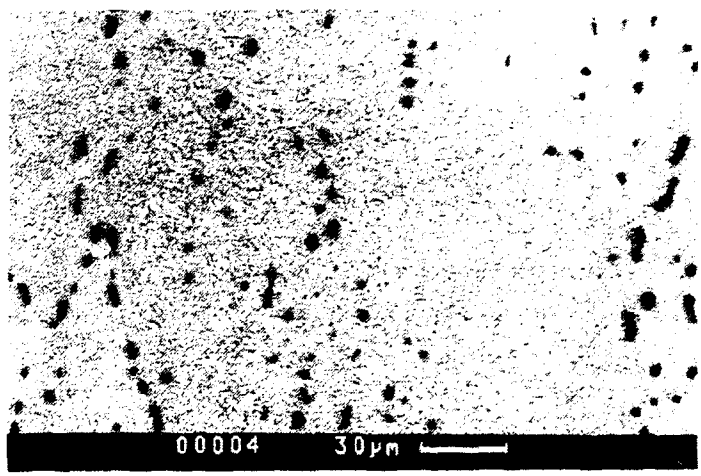
600°C / 24h



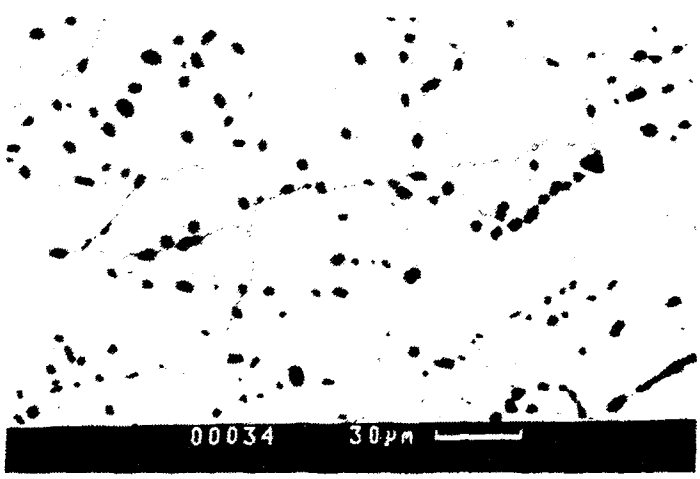
650°C / 24h



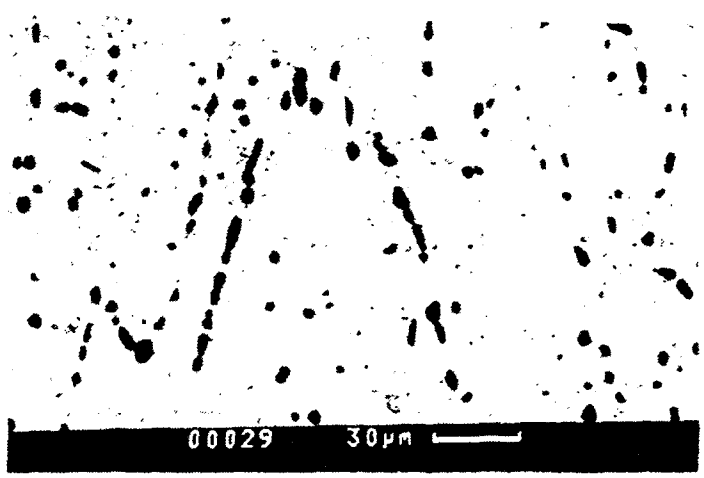
700°C / 24h



700°C / 50h

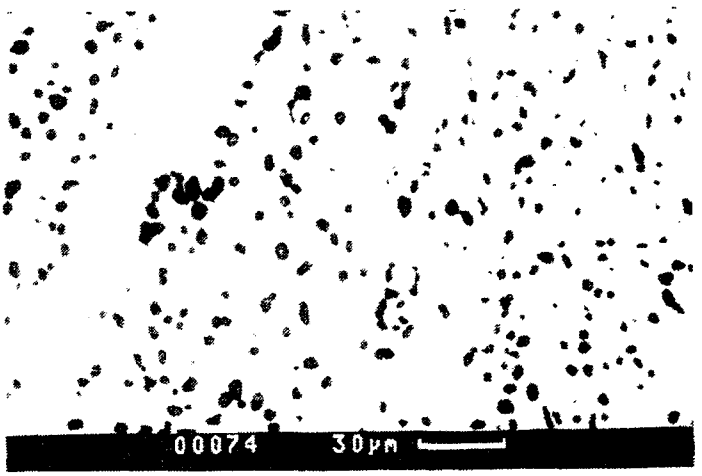


750°C / 24h

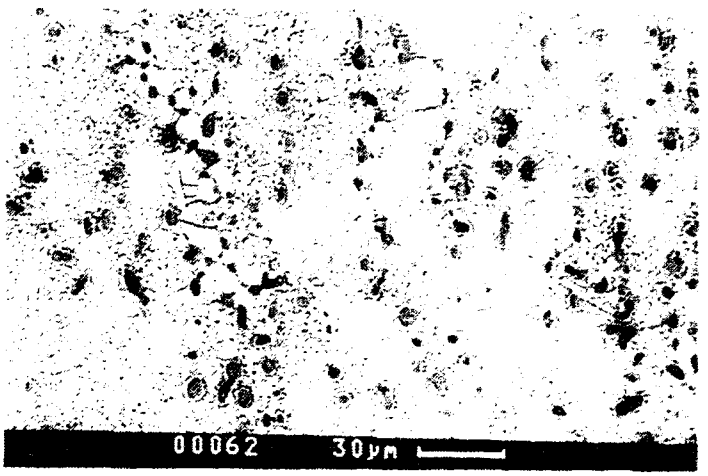


800°C / 24h

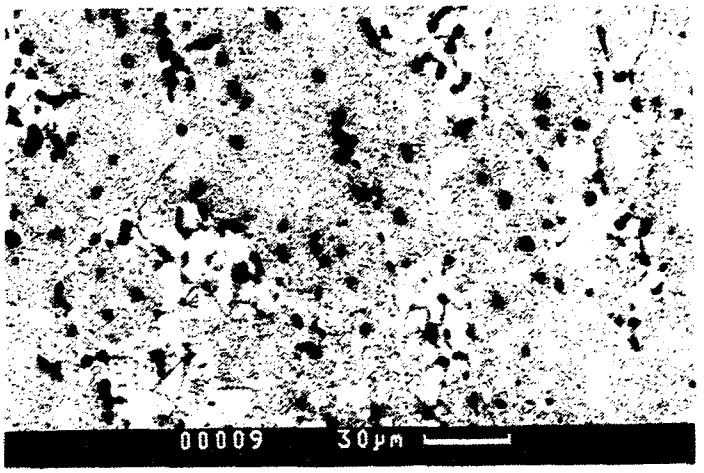
Figure 3.18; Backscattered electron images of microstructures of alloy 3 which was aged for various times and temperatures following process 1, forging plus solution treatment at 1350C / 4h.



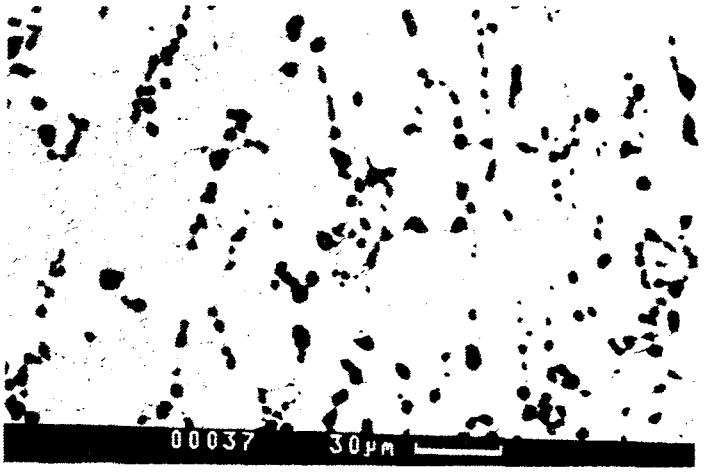
600°C / 24h



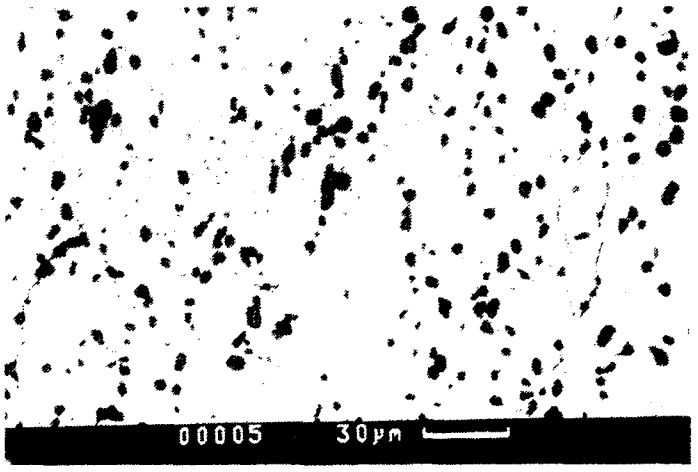
650°C / 24h



700°C / 24h

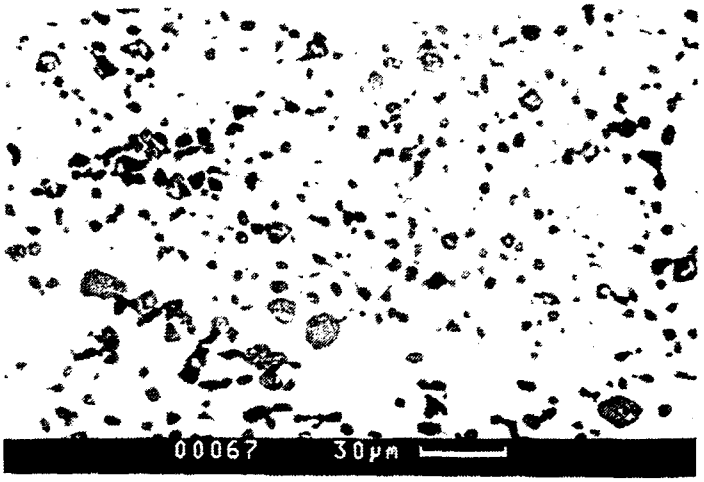


750°C / 24h

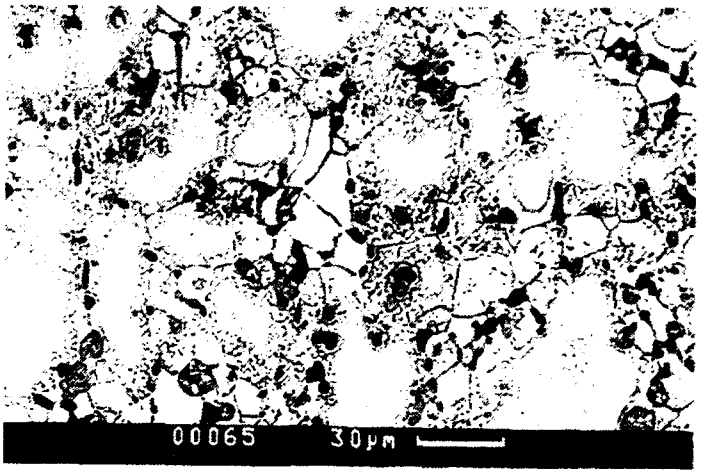


800°C / 24h

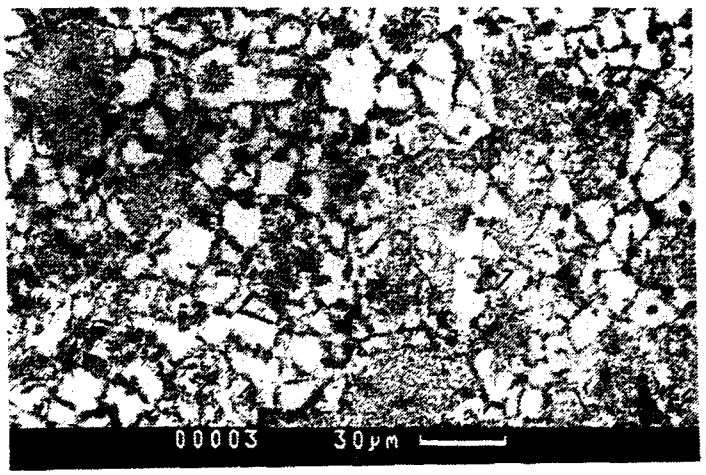
Figure 3.19; Backscattered electron images of microstructures of alloy 4 which was aged for 24h at various temperatures following process 1, forging plus solution treatment at 1350C / 4h.



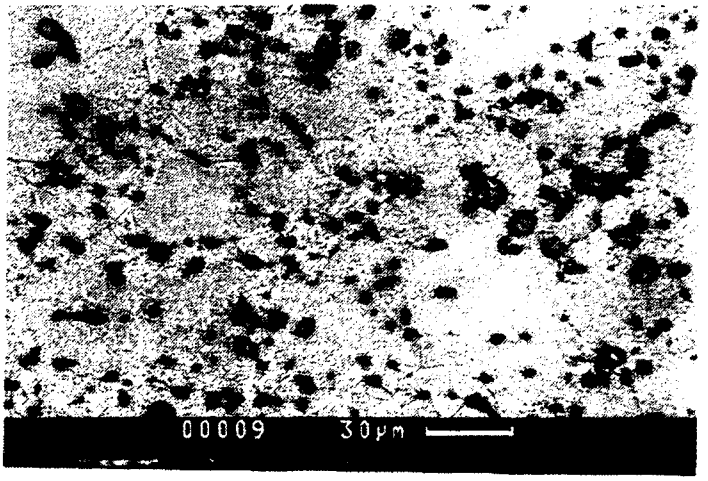
600°C / 24h



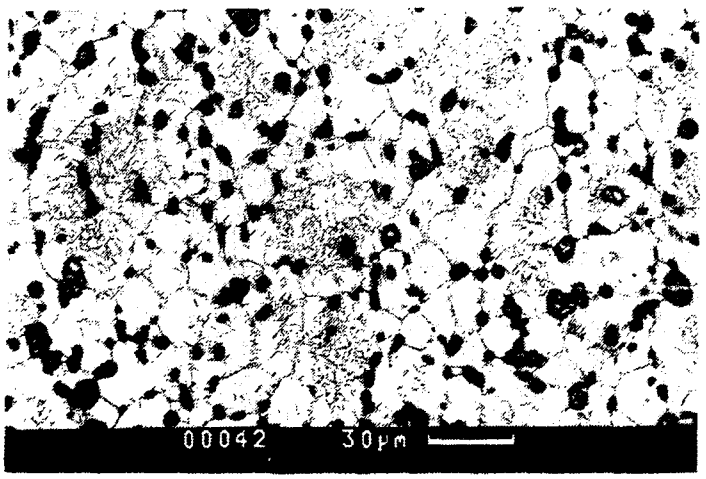
650°C / 24h



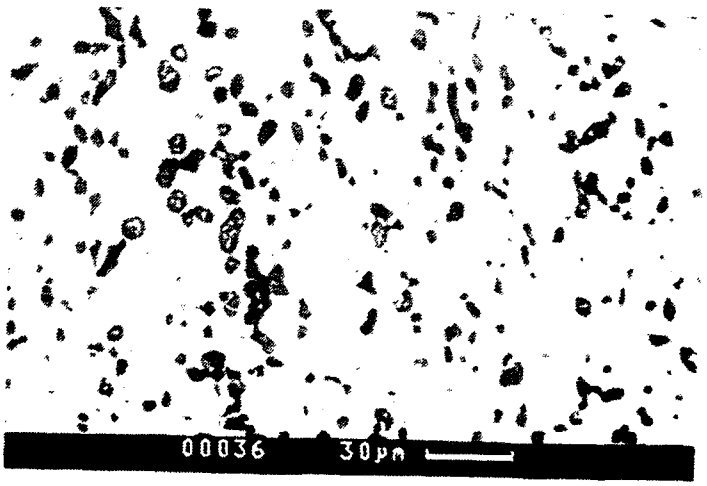
700°C / 24h



700°C / 50h

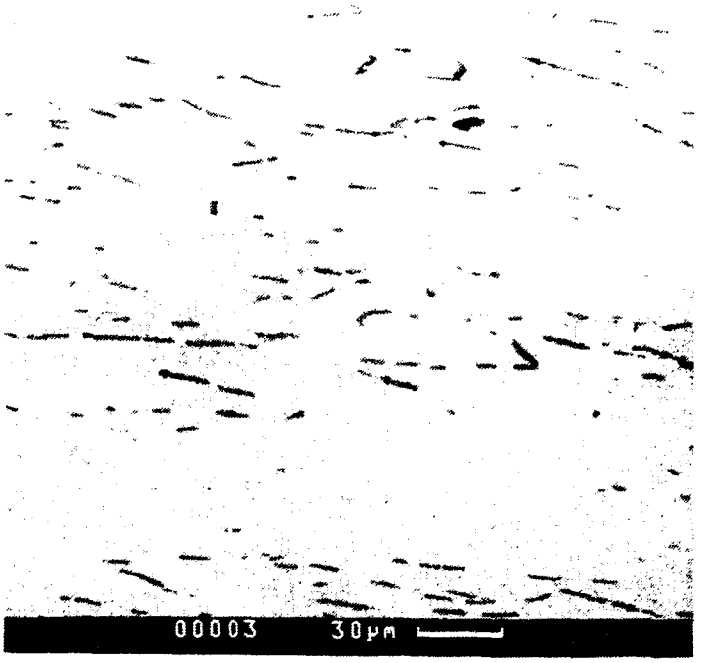


750°C / 24h

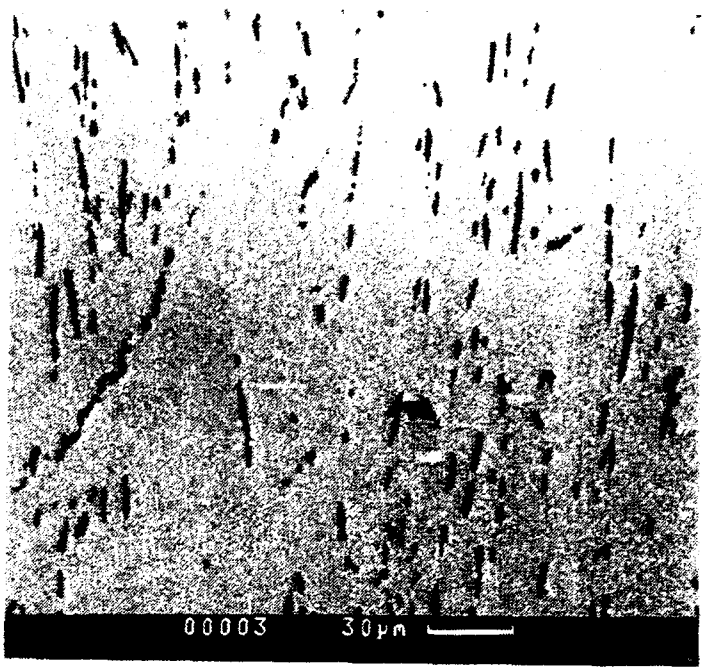


800°C / 24h

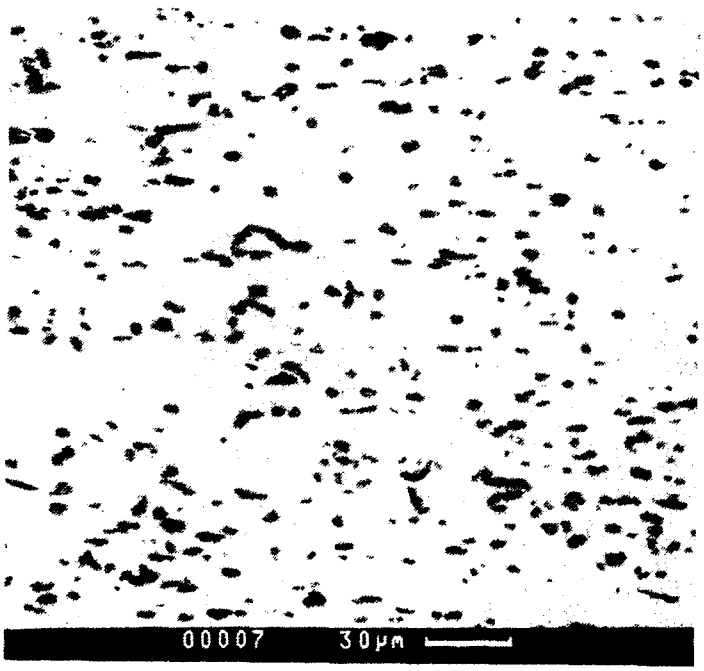
Figure 3.20; Backsc attered electron images of microstructures of alloy 5 which was aged for various times anc temperatures following process 1, forging plus solution treatment at 1350C / 4h.



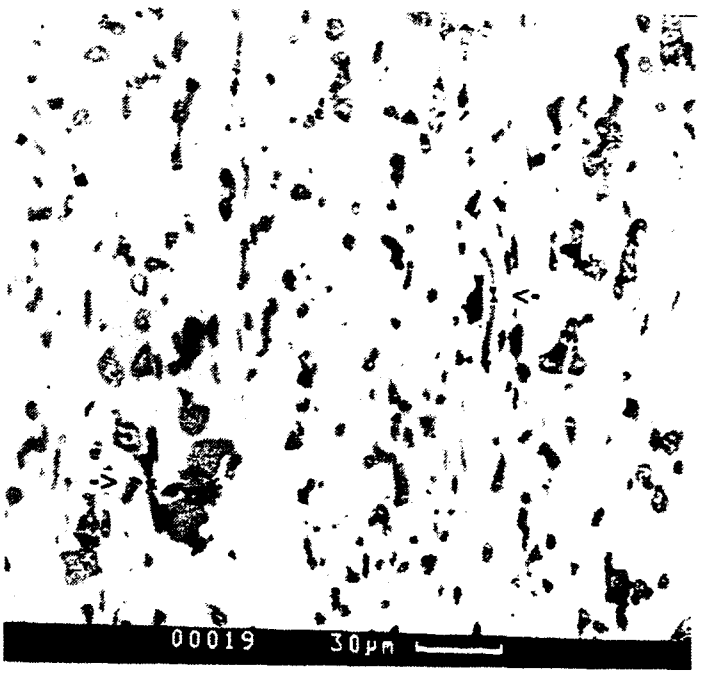
Alloy 2



Alloy 3



Alloy 4



Alloy 5

Figure 3.21; Backscattered electron images of microstructures of alloys 2 through 5 following process 2; solution treated at 1350C / 4h plus forged plus direct age at 700C / 24h. Note arrows indicate voids which were observed in high carbon alloys

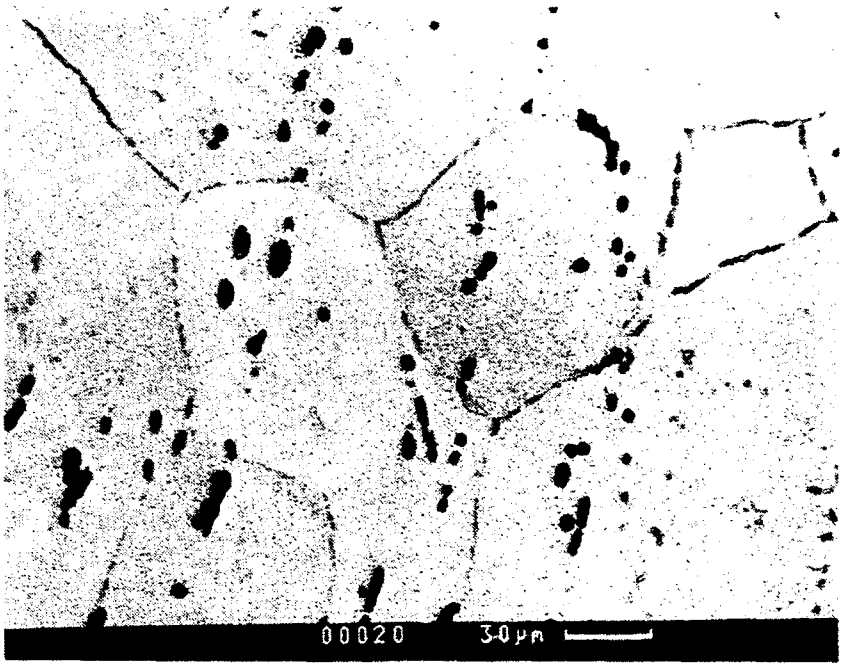


Figure 3.22; Backscattered electron images of microstructures of alloy 3 which was solution treated following process 2; solution treated at 1350C / 4h plus forged plus solution treated at 1250C / 4h.



Actual Size

Figure 3.23; Example of tensile and creep specimen which was used for testing in this program

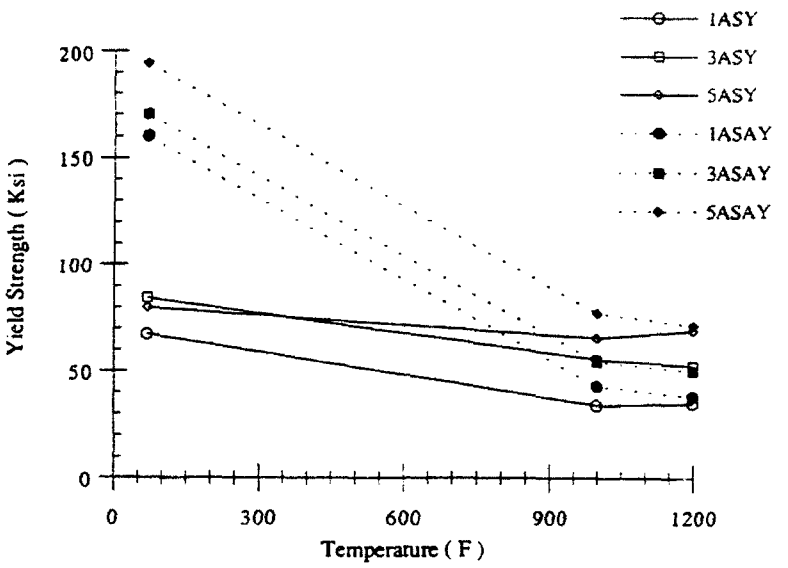


Figure 3.24; Yield strength versus temperature for alloys 1, 3, and 5 in both the solution treated (AS) and solution treated and aged (ASA) conditions indicating the increase in strength observed with increasing volume fraction of carbide.

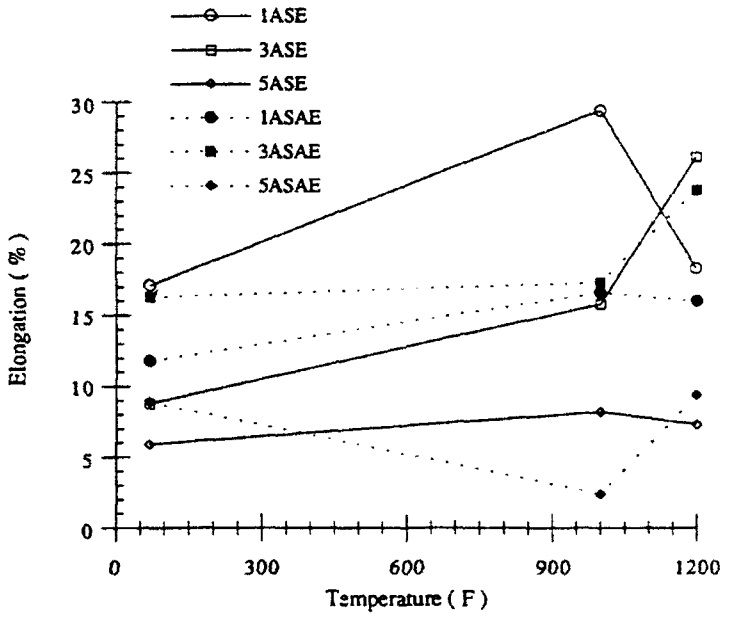


Figure 3.25; Elongation versus temperature for the same conditions in figure 3.24.

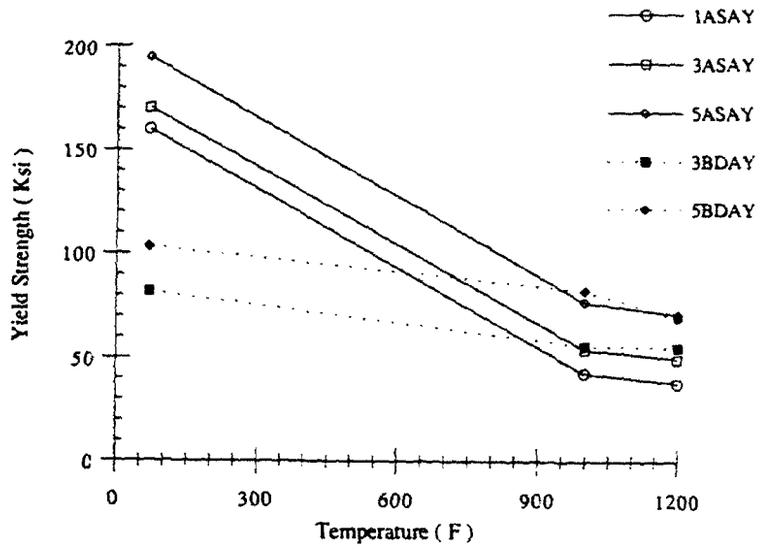


Figure 3.26; Yield strength comparison of direct age (DA) and solution and age (SA) treatments showing the higher room temperature strength achieved with solution and age

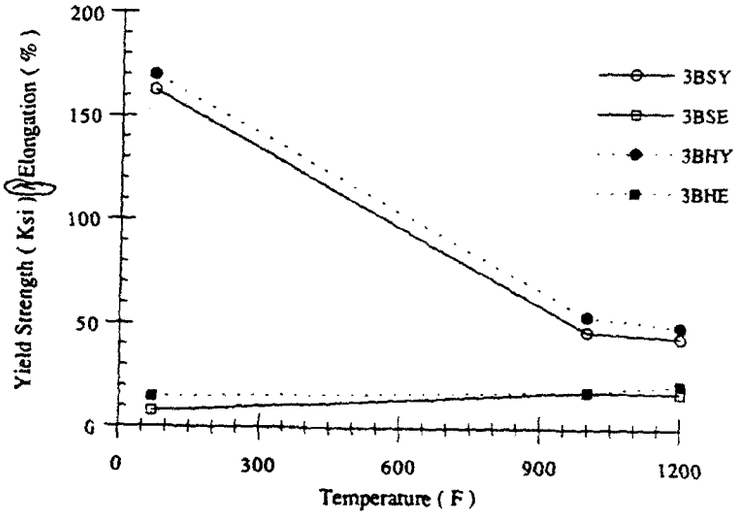


Figure 3.27; Plot of yield strength and elongation for alloy 3 showing the small increase in both yield strength and elongation for HIP'ed (H) material compared to unHIP'ed (S) material

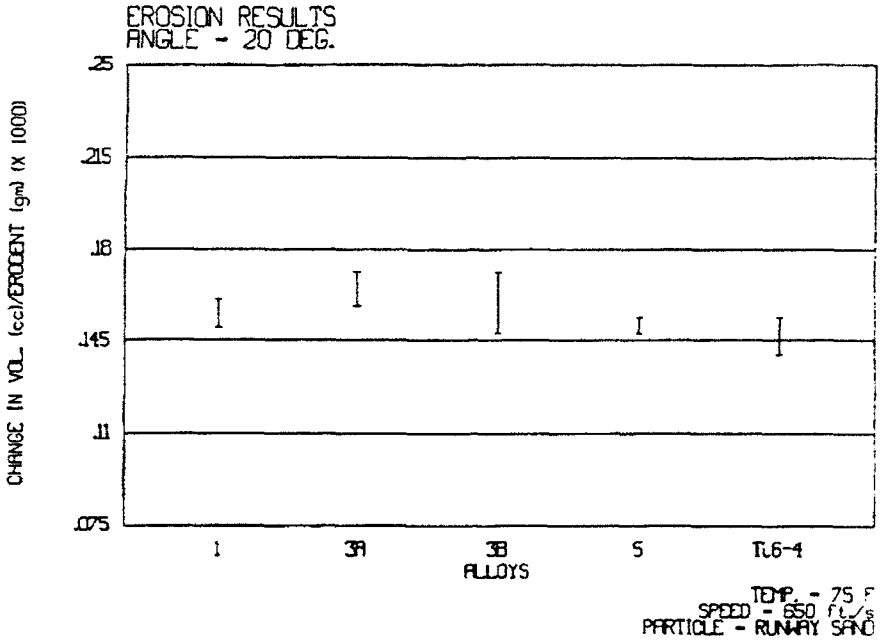


Figure 3.28; Erosion test results for a 20 degree impingement angle showing the new alloys have similar erosion resistance at this angle compared to Ti-6Al-4V

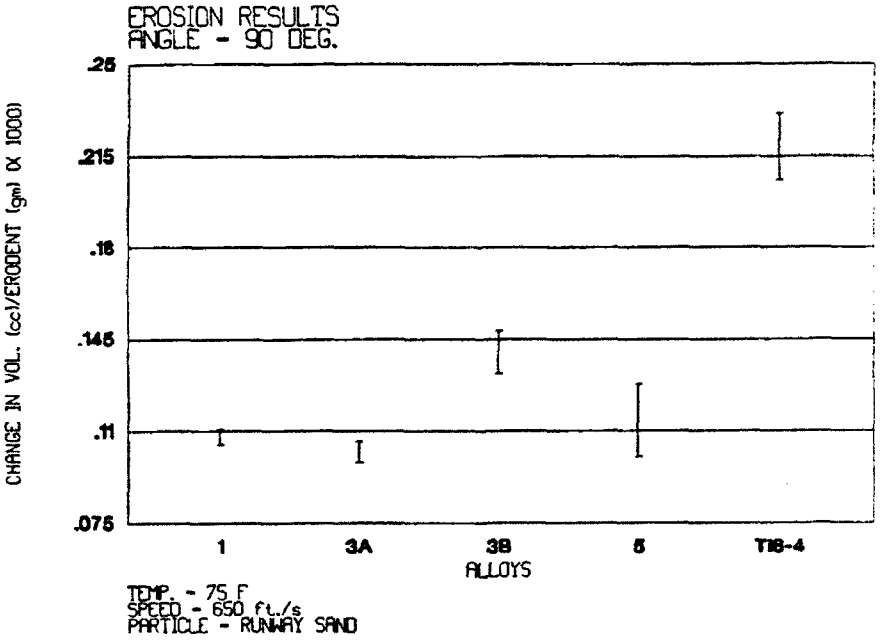


Figure 3.29; Erosion test results for a 90 degree impingement angle showing the new alloys have improved erosion resistance at this angle compared to Ti-6Al-4V